НОВИ МАТЕРИЈАЛИ
/
NEW MATERIALS IN ELECTRICAL AND ELECTRONIC ENGINEERING
(HM/NMI)

Uticaj jona retkih zemalja (Er, Yb, Ho) na karakteristike $BaTiO_3$ keramike

Vesna Paunović, *Member, IEEE*, Vojislav Mitić, Zoran Prijić, *Member, IEEE*

***Apstrakt* – U ovom radu, oksidi retkih zemalja, Er_2O_3, Yb_2O_3 i Ho_2O_3, su korišćeni kao materijali za dopiranje barijum-titanatne keramike. $BaTiO_3$ keramika dopirana je sa 0.01, 0.5 i 1.0 wt% Er, Yb ili Ho i pripremljena uobičajenim postupkom sinterovanja u čvrstom stanju. Uzorci su sinterovani na 1320 °C četiri sata. SEM analiza je pokazala da se u uzorcima $BaTiO_3$ dopiranim jonima retkih zemlje niskih koncentracija (0.01 wt%), veličina zrna kretala između 10 i 30 μm. Sa povećanjem koncentracije dopanata od 1.0 wt %, abnormalni rast zrna je zaustavljen, a veličina zrna se kretala između 2-10 μm. Merenja dielektrične konstante i dielektričnih gubitaka u zavisnosti od frekvencije i temperature vršena su u cilju uspostavljanja korelacije između mikrostrukture i dielektričnih svojstava dopirane $BaTiO_3$ keramike. Amfoterno ponašanje jona retkih zemalja dovodi do povećanja dielektrične konstante i smanjenja dielektričnih gubitaka u odnosu na nedopiranu $BaTiO_3$ keramiku. Ispitivana je i temperaturna zavisnost dielektrične konstante u zavisnosti od vrste i količine dopanata.**

Ključne reči – retke zemlje, $BaTiO_3$, dielektrična konstanta, Kirijeva temperatura, Kirijeva konstanta.

I. Uvod

Zbog visoke dielektrične konstante, temperaturne stabilnosti i malih gubitaka, elektrokeramika na bazi barijum titanata se široko koristi kao dielektrični materijal za višeslojne keramičke kondenzatore (MLCC), piezoelektrične senzore, aktuatore i DRAM memorije u integrisanim kolima [1-5]. S obzirom da su aditivi donorskog i akceptorskog tipa osnovne komponente dielektričnih materijala na bazi $BaTiO_3$, sprovedene su opsežne studije o njihovom uticaju na strukturu i svojstva $BaTiO_3$ [6-9]. Za dopiranje $BaTiO_3$ se mogu koristiti dve vrste dopanata: joni sa većim jonskim radijusima i valencom 3+ i većom koji mogu zameniti jone Ba^{2+} i joni sa manjim jonskim radijusima i valencom 5+ i većom koji mogu da zamene Ti^{4+} jone u perovskitnoj podrešetki [10-12]. U osnovi, uticaj jona dopanata na svojstva čvrstog rastvora zavisi od mesta koje dopantni jon zauzima u perovskitnoj strukturi, mehanizma kompenzacije i rastvorljivosti [13]. Pokazalo se da trovalentni joni supstituisani na Ba^{2+} lokacijama deluju kao donori, dok trovalentni joni supstituisani na Ti^{4+} lokacijama deluju kao akceptori. Kod ugradnje jona retkih zemalja u rešetku $BaTiO_3$, promena u strukturi i svojstvima $BaTiO_3$, uglavnom zavisi od mesta u rešetki gde je jon zamenjen [14].

Vesna Paunović – Univerzitet u Nišu, Elektronski fakultet, Aleksandra Medvedeva 14, 18000 Niš, Srbija (email: vesna.paunovic@elfak.ni.ac.rs).

Vojislav Mitić – Univerzitet u Nišu, Elektronski fakultet, Aleksandra Medvedeva 14, 18000 Niš, Srbija (email: vmitic.d2480@gmail.com).

Zoran Prijić – Univerzitet u Nišu, Elektronski fakultet, Aleksandra Medvedeva 14, 18000 Niš, Srbija (email: zoran.prijic@elfak.ni.ac.rs).

Joni iz sredine reda retkih zemalja, kao što su Yb^{3+}, Er^{3+}, Ho^{3+}, Dy^{3+}, Sm^{3+}, čiji su jonski radijusi po veličini između jonskih radijusa Ba^{2+} i Ti^{4+} jona, pokazuju amfoterno ponašanje i mogu zauzeti oba mesta katjonske rešetke u strukturi $BaTiO_3$ [13]. Iako neki teorijski proračuni sugerišu da će se, u širokom srednjem opsegu jonskih radijusa, trovalentni dopanti podeliti podjednako na dva mesta da bi se stvorila kompenzacija donor-akceptor [15], eksperimentalni rezultati pokazuju da se takva vrsta inkorporacije javlja u vrlo malo slučajeva [16]. Utvrđeno je da odnos Ba/Ti takođe utiče na ugradnju jona retkih zemalja u rešetku barijum titanata [17]. Ispitivanja uticaja retkih zemalja na strukturu $BaTiO_3$ pokazali su da se za odnos Ba/Ti> 1, joni Er^{3+}, Yb^{3+} ili Ho^{3+} ugrađuju na mesto Ti, a za odnos Ba/Ti <1 na mesto Ba. Štaviše, supstitucija jona retkih zemalja na mesta Ba ili Ti dovodi do neusklađenosti naelektrisanja sa rešetkom koje mora biti kompenzovano formiranjem negativno naelektrisanih defekata da bi se postigla ukupna elektroneutralnost [18]. Delimična zamena Ba^{2+} jona jonima retkih zemalja omogućava uniformnost mikrostrukture i sprečava abnormalni rast zrna.

Uzimajući u obzir da je kontrola mikrostrukture važna za optimizaciju električnih svojstava ovih materijala, u ovom radu ispitivan je uticaj Er_2O_3 i Yb_2O_3 i Ho_2O_3 na mikrostrukturu $BaTiO_3$ keramike i odgovarajuća električna svojstva.

II. Eksperimentalni deo

Uzorci su pripremljeni od komercijalnog praha $BaTiO_3$ (MURATA) i reagensa Er_2O_3, Yb_2O_3 i Ho_2O_3 u prahu (Fluka chemika). Koncentracija dopanata bila je 0.01, 0.5 i 1.0 wt% Er, Yb ili Ho. Uzorci su označeni kao 0.01Er-$BaTiO_3$ ($BaTiO_3$ dopiran sa 0.01 wt% Er) i tako dalje. Početni prah je mleven u mlinu sa kuglama u etil alkoholu tokom 24 sata koristeći boce od polipropilena i kugle od cirkonijuma. Posle nekoliko sati sušenja na 200°C, praškovi su presovani u diskove prečnika 7 mm i debljine 3 mm pod pritiskom od 120MPa. Kompakti su sinterovani na 1320°C u vazduhu tokom četiri sata. Za ispitivanje mikrostrukture uzorci su nagrizani u 10% HCl sa 5% HF. Mikrostrukture sinterovanih ili hemijski nagrizanih uzoraka posmatrane su skenirajućim elektronskim mikroskopom (JEOL-JSM 5300) opremljenim spektrometrom (EDS-QX 2000S). Raspodela veličine zrna i poroznosti uzoraka dobijena je pomoću LEICA K500MC sistema za obradu i analizu slika. Metoda linearnog merenja preseka korišćena je za procenu vrednosti veličine zrna, kao i odnosa zapremine pora. Pre električnih merenja, srebrna pasta je

nanošena na ravne površine uzoraka. Vrednosti kapaciteta i dielektričnih gubitka izmerene su pomoću Agilent 4284 LCR metra u frekvencijskom opsegu od 100Hz-20kHz. Dielektrična konstanta izračunata je iz kapacitivnosti, debljine uzorka i površine elektroda. Varijacija dielektrične konstante sa temperaturom merena je u temperaturnom intervalu od 20°C do 180°C. Dielektrični parametri izračunati su prema Kiri Vajsovom i modifikovanom Kiri Vajsovom zakonu.

.

III. REZULTATI I DISKUSIJA

A. Mikrostrukturna svojstva

Ispitivanja gustine $BaTiO_3$ dopirane keramike su pokazala da za temperaturu sinterovanja od 1320°C gustina keramike varira od 82% teorijske gustine (TD), za uzorke dopirane većom koncentracijom aditiva, do 93% TD za uzorke dopirane nižom koncentracijom, pri čemu je najveća gustina izmerena za keramiku dopiranu Ho.

SEM analiza uzoraka dopiranih Er_2O_3 ili Yb_2O_3 pokazala je da ovi uzorci imaju sličnu mikrostrukturu. Uzorci dopirani Er_2O_3 poseduju zrna nepravilnog poligonalnog oblika (slika 1), dok su u Yb dopiranom $BaTiO_3$ karakteristična zrna sfernog oblika (slika 2). Spiralni koncentrični rast zrna primećen je u uzorcima dopiranim sa 0.01 wt% Er_2O_3 i Yb_2O_3. Ovaj oblik zrna se nije pojavljivao kod uzoraka sa većom koncentracijom aditiva. Za ove uzorke formiranje „staklaste faze“ ukazalo je da je sinterovanje izvršeno u tečnoj fazi. Za najnižu koncentraciju aditiva, veličina zrna se kretala do 30 μm. Sa povećanjem koncentracije dopanata veličina zrna se smanjivala.

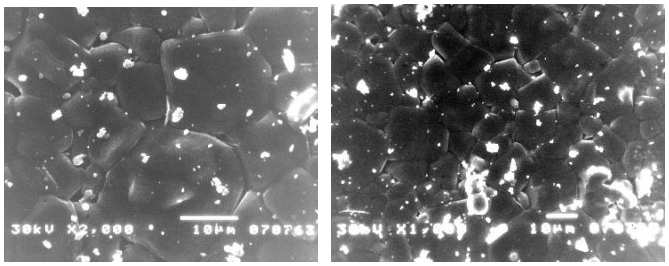

a) b)

Sl. 1 SEM mikrostruktura a) 0.01Er-$BaTiO_3$ i b) 1.0 Er-$BaTiO_3$.

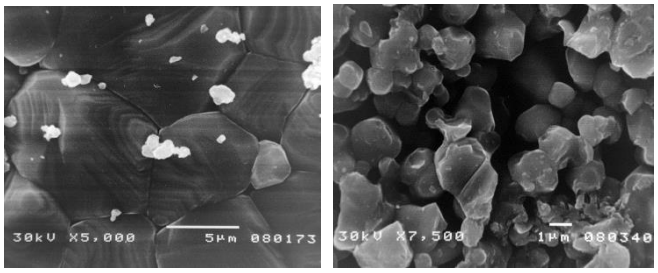

a) b)

Sl. 2. Sl. 3. SEM mikrostruktura a) 0.01Yb-$BaTiO_3$ i b) 1.0 Yb-$BaTiO_3$.

Kao rezultat toga, za uzorke sa 0.5 wt% dopanta prosečna veličina zrna bila je od 10 do 15 μm, a za uzorke dopirane sa 1.0wt% aditiva veličina zrna bila je od 2-10μm.

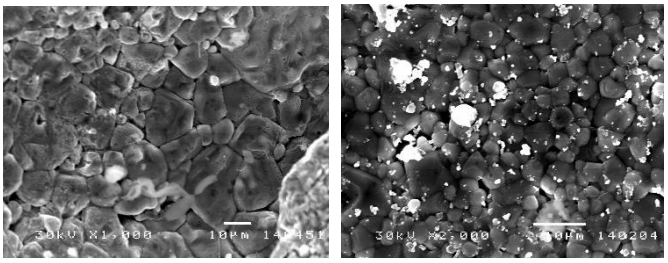

a) b)

Sl. 3. SEM mikrostruktura a) 0.01Ho-$BaTiO_3$ i b) 1.0 Ho-$BaTiO_3$.

Uzorke keramike $BaTiO_3$ dopirane Ho_2O_3 karakterišu sferna i nepravilna poligonalna zrna (sl.3). Prosečna veličina zrna za uzorke dopirane niskim sadržajem Ho_2O_3 (0.01 wt% Ho) kretala se u rasponu od 10 do 20 μm (slika 3a). Povećavanjem koncentracije dopanata veličina zrna se smanjuje i za uzorke dopirane sa 0.5 wt% Ho veličina zrna se kretala od 2 μm do 10 μm, a za uzorke dopirane sa većom koncentracijom dopanata (1.0 wt% Ho) prosečna veličina zrna je bila od 2 μm do 3 μm (slika 3b).

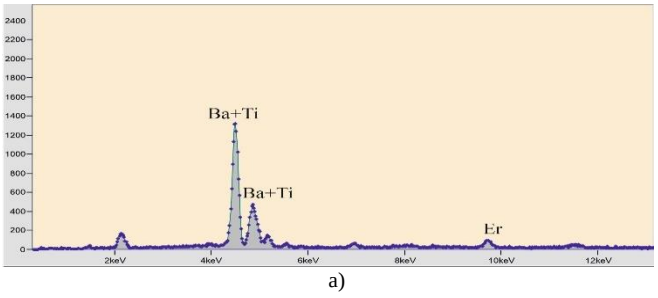

a)

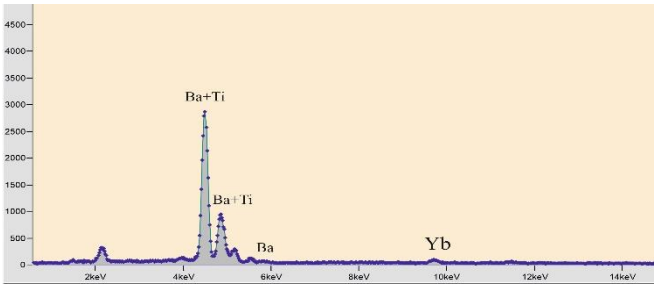

b)

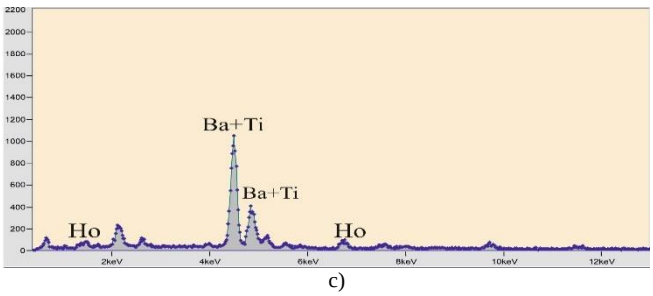

c)

Sl. 4. EDS spektar a) Er-$BaTiO_3$, b) Yb-$BaTiO_3$ i c) Ho-$BaTiO_3$.

EDS analiza uzoraka dopiranih sa 0.01 wt.% dopanata nije pokazala postojanje oblasti bogatih Er, Yb ili Ho što je

ukazivalo na uniformnu ugradnju dopanata u uzorke. Povećanje koncentracije dopanata dovelo je do pojave regiona bogatih Er između zrna kao i regiona bogatih Ho i Yb za koje je karakteristična sitnozrnasta mikrostruktura (slika 4).

Rentgenska analiza (XRD) uzoraka pokazala je samo $BaTiO_3$ perovskitnu fazu i ravnomernu raspodelu aditiva.

B. Električna svojstva

Uticaj koncentracije aditiva i dobijene mikrostrukture na dielektrične osobine uzoraka dopiranih jonima retkim zemalja se može ispitati zavisnošću dielektrične konstante i dielektričnih gubitaka od temperature i frekvencije (slike 5, 6 i 7). Frekventni opseg za sve ispitivane uzorke kretao se od 100Hz do 20kHz dok je temperaturni opseg bio od 20°C do 180°C.

Tok promene dielektrične konstante sa frekvencijom je isti u svim uzorcima. Dielektrična konstanta nakon neznatno većih vrednosti na niskim frekvencijama opada i postaje gotovo konstantna za frekvencije veće od 3KHz.

Dielektrična konstanta ispitivanih uzoraka kretala se od 614 do 2100 na sobnoj temperaturi (Tabela I). Za 0.01-Er dopirani $BaTiO_3$ dielektrična konstanta iznosi 1200, a za 0.01-Yb-$BaTiO_3$, i 0.01-Ho-$BaTiO_3$ dielektrična konstanta iznosi 1150 i 2100 respektrivno. Generalno, uzorci $BaTiO_3$ dopirani Ho pokazuju najveću dielektričnu konstantu u poređenju sa Er-$BaTiO_3$ i Yb –$BaTiO_3$ uzorcima.

Vrednosti dielektričnih gubitaka (*tan δ*) bile su u opsegu od 0.01-0.15. Glavna karakteristika svih uzoraka je da se nakon početno većih vrednosti dielektričnih gubitaka, *tan δ* smanjuje i gotovo je nezavisan od frekvencije pri frekvencijama većim od 5 kHz, što je prikazano na slici 6. Smanjenje *tan δ* u frekvencijskom opsegu od 100Hz-20 kHz može se povezati sa smanjenjem električne otpornosti uzoraka sa 10^6 Ωcm na 100 Hz na 10^2 Ωcm na 20 kHz.

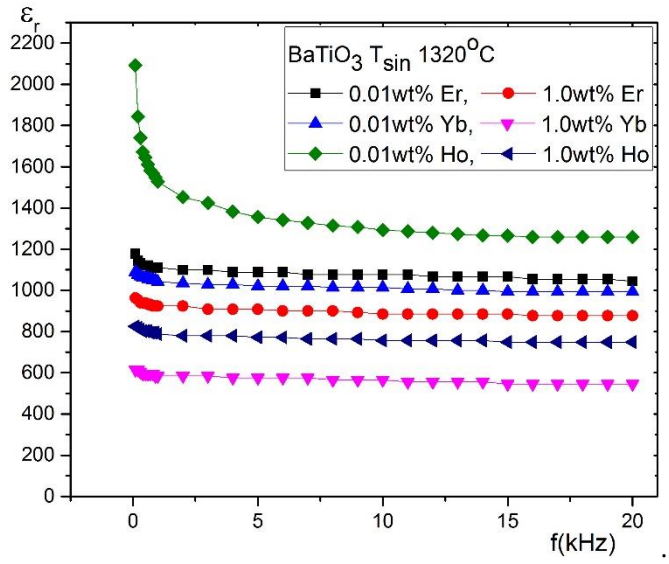

Sl. 5. Zavisnost dielektrične konstante od frekvencije.

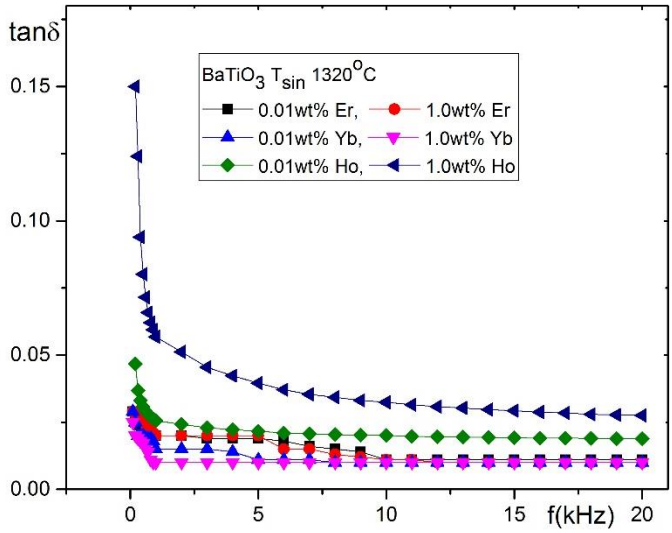

Sl. 6. Zavisnost dielektričnih gubitaka od frekvencije.

Uticaj tipa aditiva i karakteristika mikrostrukture na dielektrično ponašanje Er, Yb i Ho dopiranog $BaTiO_3$ može se proceniti pomoću krivih zavisnost permitivnosti od temperature (slika 7). Najveća promena dielektrične konstante u odnosu na temperaturu za uzorke sa niskom koncentracijom aditiva (0.01 wt%) primećena je u Yb dopiranom $BaTiO_3$ za koji je dielektrična konstanta na Kirijevoj temperaturi 5453. Relativno stabilan odziv dielektrične konstante u funkciji temperature do 100°C primećen je u svim dopiranim uzorcima. Sa većom koncentracijom aditiva (1.0 wt%), primećena je mala promena dielektrične konstante sa temperaturom u celom temperaturnom intervalu kod svih uzoraka. Smanjenje dielektrične konstante u dopiranim uzorcima sa porastom koncentracije dopanata, može se pripisati s jedne strane segregaciji dopanata, a sa druge strane smanjenju gustine uzoraka sa 93 na 82% TG. Kirijeva temperatura (T_C) na kojoj je vrednost ε_r maksimalna, niža je od vrednosti T_C za čisti $BaTiO_3$ i kretala se u opsegu od 122°C do 129°C.

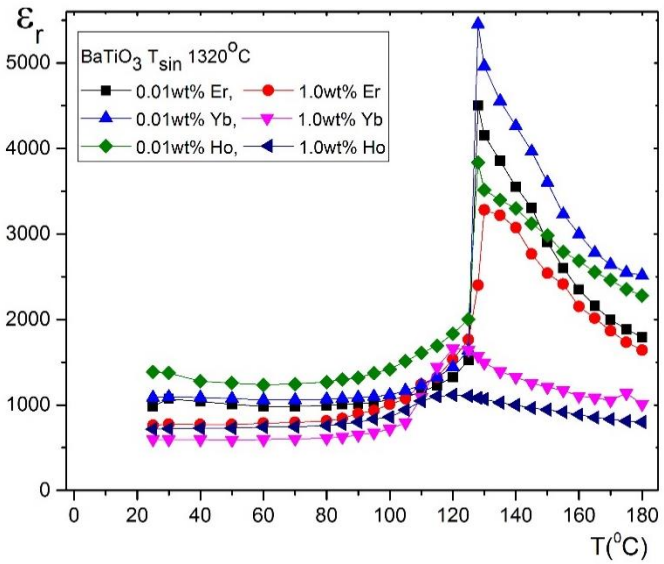

Sl. 7. Zavisnost dielektrične konstante od temperature.

Dielektrična konstanta u feroelektriku raste sa temperaturom, dostiže maksimalnu vrednost na Kirijevoj temperaturi i opada sa daljim porastom temperature. Zavisnost dielektrične permitivnosti od temperature u paraelektričnom regionu, tj. u području iznad Kirijeve temperature, može se opisati Kiri-Vajsovim zakonom.

Fitovanjem zavisnosti recipročne vrednosti dielektrične konstante od temperature, kao što je prikazano na slici 8, dobijaju se vrednosti Kiri-Vajsove temperature T_0. Ova temperatura ima nižu vrednost od Kirijeve temperature T_C za sve izmerene uzorke. Najviša vrednost za T_0 dobijena je za uzorke dopirane sa 0.01 wt% Er (T_0 = 97°C), a najniža vrednost T_0 za uzorke dopirana sa 1.0 wt% Ho (T_0 = 10°C). U tabeli I date su vrednosti Kiri-Vajsove temperature za sve ispitivane uzorke.

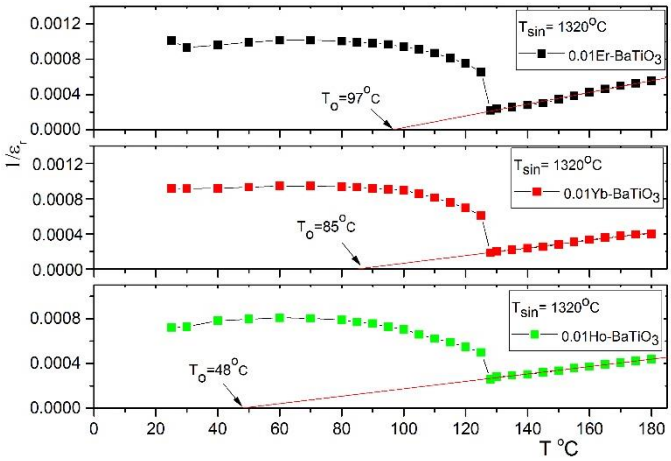

Sl. 8. Recipročna vrednost dielektrične konstante u funkciji temperature.

Na osnovu Kiri-Vajsovog zakona izračunavaju se vrednosti Kirijeve konstante C za sve izmerene uzorke. Vrednost Kirijeve konstante opada sa porastom koncentracije aditiva tako da se najveća vrednost izračunava za uzorke sa koncentracijom aditiva 0.01 wt% ($3.04\cdot10^5$ K za Ho-$BaTiO_3$, $2.34\cdot10^5$K za Yb-$BaTiO_3$ i $1.53\cdot10^5$ K za Er-$BaTiO_3$), a najmanja za uzorke sa koncentracijom aditiva 1.0 wt%. Uzorke sa najvećom vrednošću C karakterišu krupnozrna mikrostruktura i veća gustina. Vrednosti za Kirijevu konstantu u skladu su sa promenom gustine ispitivanih uzoraka, kao i sa mikrostrukturnim karakteristikama.

Za sve izmerene uzorke karakterističan je oštar prelaz iz feroelektrične u paraelektričnu oblast, kao i nagli porast dielektrične permitivnosti na Kirijevoj temperaturi. Ova činjenica se može potvrditi odnosom dielektrične konstante na Kirijevoj temperaturi (ε_{rmax}) i na sobnoj temperaturi (ε_{rmin}), tj. (ε_{rmax} / ε_{rmin}). Najviši odnos dielektrične konstante izračunat je za uzorke dopirane sa 0.01 wt% (od 4.74 za 0.01-Yb-BaTiO do 1.61 za 0.01-Ho-$BaTiO_3$), a najmanji odnos uzoraka dopirane sa 1.0wt%.

Pored Kiri-Vajsovog zakona za ispitivanje ponašanja feroelektrika u paraelektričnoj fazi koriste se i modifikovani Kiri-Vajsov zakon koji opisuju odstupanja od linearnosti $\varepsilon_r = f(T)$ usled difuzne fazne transformacije:

$$\frac{1}{\varepsilon_r} = \frac{1}{\varepsilon_{r\max}} + \frac{(T - T_{\max})^{\gamma}}{C'}. \qquad (1)$$

gde je C' konstanta slična Kirijevoj konstanti, γ - kritični eksponent nelinearnosti koji pokazuje odstupanje od linearne zavisnosti ε_r od temperature u paraelektričnoj oblasti. Na osnovu fitovanja krivih $ln(1/\varepsilon_r - 1/\varepsilon_{rmax})$ u funkciji $ln(T-T_{max})$, γ je dobijen kao nagib krive.

Vrednost kritičnog eksponenta nelinearnosti γ za izmerene uzorke kreće se od 1.02 za uzorke dopirane 0.01wt% Ho do 1.19 za uzorke dopirane 1.0wt% aditiva (Tabela I). Vrednost γ raste sa povećanjem koncentracije aditiva. Ove vrednosti su u skladu sa eksperimentalnim podacima, jer je za ove uzorke karakterističan oštar prelaz iz feroelektričnog u paraelektrični region što ukazuje na strukturnu faznu transformaciju.

TABELA I
DIELEKTRIČNI PARAMETRI ZA ISPITIVANE UZORKE

Uzorci $BaTiO_3$	ε_r na T=300K	ε_r na T_C	T_c [°C]	T_0 [°C]	$C\cdot10^5$ [K]	γ
0.01wt %Er	1200	4505	128	97	1.53	1.12
0.5wt%Er	1199	4100	128	87	1.24	1.18
1.0wt%Er	1010	3281	129	85	1.65	1.19
0.01wt%Yb	1150	5453	128	85	2.34	1.11
0.5wt%Yb	614	1660	125	28	1.55	1.15
1.0wt%Yb	610	1657	125	27	1.48	1.19
0.01wt%Ho	2100	3834	128	48	3.04	1.02
0.5wt%Ho	800	1290	125	25	1.62	1.14
1.0wt%Ho	700	1117	122	10	1.54	1.17

IV. ZAKLJUČAK

U ovom radu su predstavljena ispitivanja uticaja jona retkih zemalja, kao što su Yb_2O_3, Er_2O_3 i Ho_2O_3 na mikrostrukturu $BaTiO_3$ keramike i odgovarajuća električna svojstva. Naša ispitivanja su pokazala da za temperaturu sinterovanja od 1320°C gustina keramike varirala od 82% teorijske gustine (TD), za uzorke dopirane većom koncentracijom dopanata do 93% TD za uzorke sa niskom koncentracijom dopanata. Primećeno je da povećanje sadržaja katjona retkih zemljanih sprečava abnormalni rast zrna. Prosečna veličina zrna u uzorcima dopiranim sa malim sadržajem aditiva kretala se između 10-30 μm, a kod 1.0 wt% od 2-10 μm. Dielektrična merenja su pokazala da, generalno, uzorci Ho-$BaTiO_3$ pokazuju najveću vrednost dielektrične konstante na sobnoj temperaturi a da su najveće promene dielektrične konstante sa temperaturom zabeležene kod Yb-$BaTiO_3$ uzoraka. Dielektrična konstanta ispitivanih uzoraka kretala se od 610 do 2100 na sobnoj temperaturi. Smanjenje dielektrične konstante sa povećanjem koncentracije dopanata

povezano je sa neujednačenom raspodelom dopanata u strukturi perovskita. Svi uzorci imaju oštar fazni prelaz i slede Kiri-Vajsov zakon. Kirijeva konstanta (*C*) opada sa povećanjem količine aditiva za sve vrste uzoraka. Kritični eksponent γ je u rasponu od 1.02 do 1.19 i povećava se sa porastom koncentracije aditiva. Dobijeni rezultati omogućavaju dalju optimizaciju električnih svojstava materijala na bazi barijum-titanata, posebno sa stanovišta sinteze-struktura-svojstva.

ZAHVALNICA

Ovaj rad je podržalo Ministarstvo prosvete, nauke i tehnološkog razvoja Republike Srbije (Ev. br. 451-03-9/2021-14/200102).

LITERATURA

[1] S.Wang, G.O.Dayton "Dielectric Properties of Fine-Grained Barium Titanate Based X7R Materials" *J. Am. Ceram. Soc.* 82 [10], pp 2677–2682, 1999.

[2] C.Pithan, D.Hennings, R. Waser "Progress in the Synthesis of Nanocrystalline $BaTiO_3$ Powders for MLCC" *International Journal of Applied Ceramic Technology* 2 [1], pp.1–14, 2005.

[3] Y. Lu, H. Haoa, S. Zhang, H. Liu, C. Su, Z. Yao, M. Cao, J " Microstructure and dielectric characteristics of Nb_2O_5 doped $BaTiO_3$-$Bi(Zn_{l/2}Til_{/2})O_3$ ceramics for capacitor applications", . E. Ceram. Soc., 37, pp. 123-128, 2017.

[4] J.Nowotny, M.Rekas "Positive temperature coefficient of resistance for $BaTiO_3$-based materials" *Ceram. Int*., 17 [4], pp. 227-41, 1991.

[5] C.Metzmacher, K.Albertsen, "Microstructural Investigations of Barium Titanate-Based Material for Base Metal Electrode Ceramic Multilayer Capacitor" J.Am.Ceram.Soc. 84 [4], pp. 821-26, 2004.

[6] D.H. Kuo, C.H.Wang, W.P.Tsai, ″Donor and acceptor cosupstitued $BaTiO_3$ for nonreducible multilayer ceramic capacitors″, Ceram. Int. vol. 32, pp. 1-5, 2006.

[7] V. Paunovic, V. V. Mitic, Lj. Kocic, ″Dielectric characteristics of donor-acceptor modified $BaTiO_3$ ceramics″, Ceram. Int. vol. 42, no. 10, pp. 11692-11699, 2016.

[8] N.H.Chan, D.M.Smyth, "Defect chemistry of donor-doped $BaTiO_3$" *J. Am. Ceram. Soc*., 67 [4] pp. 285-8 1984.

[9] D.ltzke, H.Abicht, "The influence of different additives and the mode of their addition on the sintering behavior and the properties of semiconducting barium titanate ceramics" *Solid State Sciences* 2, pp.149–159, 2000.

[10] V. Paunovic, V. V. Mitic, M. Miljkovic, V. Pavlovic, Lj. Živkovic, ″Ho_2O_3 Additive Effects on $BaTiO_3$ Ceramics Microstructure and Dielectric Properties″ *Science of. Sintering*, vol. 44, no. 2, pp. 223-233, 2012.

[11] H.M.Chan, M.P.Hamer, D.M.Smyth, "Compensating defects in highly donor-doped $BaTiO_3$" *J.Am. Ceram. Soc*., 69 [6] 507-10, 1986.

[12] P.W.Rehrig, S.Park, S.Trolier-McKinstry, G.L.Messing, B.Jones, T.Shrout "Piezoelectric properties of zirconium-doped barium titanate single crystals grown by templated grain growth" *J. Appl. Phys.* 86 [3], 1657-1661, 1999.

[13] D.Makovec, Z.Samardzija M.Drofenik "Solid Solubility of Holmium, Ytrium and Dysprosium in $BaTiO_3$" *J.Am.Ceram.Soc.*, 87 [7], pp. 1324-1329 (2004).

[14] D.Lu, X.Sun, M.Toda, "Electron Spin Resonance Investigations and Compensation Mechanism of Europium-Doped Barium Titanate Ceramics" *Japanese Journal of Applied Physics* 45 [11] pp.8782-8788 (2006).

[15] M. T. Buscaglia, V. Buscaglia, P. Ghigna, M. Viviani, G. Spinolo, A. Testino and P. Nanni, "Amphoteric behaviour of Er^{3+} dopants in $BaTiO_3$: an Er–L_{III} edge EXAFS assessment" *Phys. Chem. Chem. Phys.*, 6**,** pp. 3710, 2004.

[16] G.V. Lewis, C.R.A. Catlow, " Defect studies of doped and undoped barium titanate using computer simulation techniques" *J. Phys. Chem. Solids* 47 pp. 89-97, 1986.

[17] L.Xue, Y.Chen, R.Brook, "The influence of ionic radii on the incorporation of trivalent dopants into $BaTiO_3$" *Materials Sci. and Eng. B* Vol. 1 2, pp. 193-201, 1988.

[18] John D. Bak, John C. Wright "Site-Selective Spectroscopy of the Solid-State Defect Chemistry in Erbium-Doped Barium Titanate" *J. Phys. Chem. B, 109*, 18391-18399, 2005.

ABSTRACT

In this paper, rare earth oxides, Er_2O_3, Yb_2O_3, and Ho_2O_3, were used as doping materials for barium titanate ceramics. $BaTiO_3$-ceramics were prepared by a conventional solid-state reaction method. The concentration of additives was 0.01, 0.5, and 1.0 wt%. The samples were sintered at 1320°C for four hours. In $BaTiO_3$ samples doped with rare-earth ions of low concentrations (0.01 wt%), the grain size ranged between 10 and 30 μm. With an increase in dopant concentration of 1.0 wt%, abnormal grain growth was inhibited, and grain size ranged between 2-10μm. Measurements of dielectric constant and dielectric losses as a function of frequency and temperature were performed to establish a correlation between the microstructure and dielectric properties of doped $BaTiO_3$ ceramics. The amphoteric behavior of rare-earth ions leads to an increase in the dielectric constant and a decrease in dielectric losses in relation to undoped $BaTiO_3$ ceramics. The temperature dependence of the dielectric constant in function on the type and concentration of dopants was also investigated.

Influence of rare earth ions (Er, Yb, Ho) on the $BaTiO_3$ ceramics characteristics

Vesna Paunović, Vojislav Mitić, Zoran Prijić

Mössbauer Spectroscopy of Iron-based Chalcogenides

Valentin N. Ivanovski

Abstract*—Soon after the discovery of superconductivity in LaFeAsO with T_C = 26 K in 2008, many other iron-based superconductors were synthetized. They are all based on the layers which contain iron and a pnictogen (As, P) or a chalcogen (S, Se, Te) element. Due to the connection between superconductivity and magnetism these novel unconventional high-T_C superconductors have attracted tremendous interest in the scientific community. A particularly well studied is tetragonal FeSe in the PbO type structure (11 family). The improvement of T_C was achieved by the intercalation of an additional layer such as perovskite-like blocks or alkaline metals into the Fe-based chalcogenide layered systems. This led to creation of new superconducting compounds, $A_yFe_{2-x}Se_2$ (*A* is an alkaline element) named 122 family whose physical and structural properties are found to be very sensitive on details of the chemical composition. Unlike layered cuprate superconductors, a cationic disorder arisen from a substitution in an Fe-layer improves T_C. The highest T_C in the Fe-based chalcogenide superconductors is accomplished by suppression of both long range crystallographic and magnetic order. Mössbauer spectroscopy is a very useful tool for studies of structural phase transitions, structure defects, and chemical and structural inhomogeneities. This lecture is devoted to the local structure studies of $FeSe_xS_{1-x}$, $K_{0.7}Na_{0.1}Fe_2Se_2$, $KFe_{1-x}Co_xSe_2$, and similar Fe-based chalcogenide compounds using the Mössbauer spectroscopy.

***Index Terms*—Superconductors; iron-based chalcogenides; Mössbauer spectroscopy; local structures.**

Valentin N. Ivanovski is with the "Vinča" Institute of Nuclear Sciences - National Institute of the Republic of Serbia, University of Belgrade, P.O.Box 522, 11001 Belgrade, Serbia (e-mail: valiva@vin.bg.ac.rs).

An Overview on a Graph Theory Applications New Frontiers in Electronics Materials

Vojislav V.Mitic, Branislav Randjelovic, Dusan Milosevic, Srdjan Ribar, Ivana Radovic, Markus Mohr and Hans Jorg Fecht

***Abstract* — This paper are new exciting results and an overview in graph theory applications on various problems in electronic materials. This opens new frontiers in this field. There are a lot of scientific efforts, especially during last few years. Our research team made very significant contribution, particulary related to calculation of parameters of BaTiO3 ceramics, calculation of syntetized diamonds electrophysical parameters, modelling of microeletronic intergranular relations and use of materials in medicine, based on biomimetic. We also discuss interesting possibilities for further research.**

***Index Terms* — graph theory; nanostructures; ceramics.**

I. Introduction

Graph theory application in synthesis of ceramic materials with control on phenomena between the grains is very challenging (see [1-5]), especially combined or compared with fractals and neural networks applications. It could enable design of the material with specific functionalities and widen the field and conditions for their application. Properties on the grain boundary can be calculated and analyzed based on the values measured on bulk materials samples (for methods of measurement see [1,3,4,5,8]). Possibility of using graph theory for determination of dielectric properties at the grain boundary of modified $BaTiO_3$ ceramics, based on the properties measured on the bulk samples is shown. This opens completely new perspectives in the area of miniaturization and micropackaging, because electrical-electronic-dielectric parameters values are calculated on a micro level (see [3, 6-9]).

Vojislav V.Mitić is with Faculty of Electrical Engineering, University of Nis, 14 Aleksandra Medvedeva, 18000 Belgrade, Serbia (e-mail: vmitic.d2480@gmail.com).

Branislav M.Randjelović is with Faculty of Electrical Engineering, University of Nis, 14 Aleksandra Medvedeva, 18000 Belgrade, Serbia (e-mail: bane@elfak.ni.ac.rs).

Dusan Milosević is with Faculty of Electrical Engineering, University of Nis, 14 Aleksandra Medvedeva, 18000 Belgrade, Serbia (e-mail: dusan.milosevic@elfak.ni.ac.rs).

Srdjan Ribar is with Faculty of Mechanical Engineering, University of Belgrade, Kraljice Marije 16, 11120 Belgrade Serbia, Belgrade, Serbia (e-mail: srdjanribar@gmail.com).

Ivana Radovic is with Institute of Nuclear Sciences 'VINČA', University of Belgrade, Mike Petrovica Alasa 12-14, 11000 Belgrade, Serbia (e-mail: ivanaradovic.80@gmail.com).

Markus Mohr is with University of Ulm, Institute of Functional Nanosystems, Ulm, Germany (e-mail: markus.mohr@uni-ulm.de).

Hans J. Fecht is with University of Ulm, Institute of Functional Nanosystems, Ulm, Germany (e-mail: hans.fecht@uni-ulm.de).

II. Graph Theory in Intergranular Relations

We have 3D structure of synthesized electronic material that should be presented or modelled using graph theory for calculation of parameters at grain boundary ([2]), shown on Fig.1. Let us consider 1D and 2D case, because this 2D case could be, later, easily generalized and mapped onto some 3D case.

A. Modelling with 1D and 2D graphs

In order to establish appropriate theoretical experiment, through which we will model this sintered plate with graph [2], lets simplify, and instead of 2D case (Fig.2), we will take one of 1D cases (Fig.3):

Fig. 1. Structure of grains (3D case)

Fig. 2. Structure of grains according to 2D case

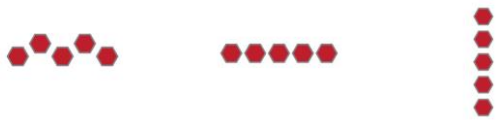

Fig. 3. Structure of grains according to 1D case

Now, let us make graph from one of those cases, for example the last one (vertical arrangement) with n=5 grains. Our goal is to get overall results in change of capacitance, in relation with those (measured) overall results. So, we have graphs, shown on Fig.4 (see [5]).

If we use experimental results from [5] and divide overall capacitance change to a local measure, between two grains, for example, for n=5 and for DC bias 25V, we have overall

capacity change 69.45. This means that between neighboring vertices in graph we have capacity change $\frac{\Delta C}{C}$ of

$$\frac{\Delta C}{C} = 69.45 / (n-1) = 69.45 / 4 = 17.3625$$

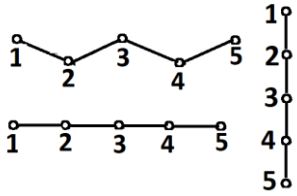

Fig. 4. Modelling with 1D graphs

Appropriate matrix of this graph (for n=5) is

$$A = \begin{bmatrix} 0 & 17.3625 & 0 & 0 & 0 \\ 17.3625 & 0 & 17.3625 & 0 & 0 \\ 0 & 17.3625 & 0 & 17.3625 & 0 \\ 0 & 0 & 17.3625 & 0 & 17.3625 \\ 0 & 0 & 0 & 17.3625 & 0 \end{bmatrix}$$

In that case, we have parallel connection of capacity changes, and overall capacity change is equal to 68.73 (see [10]).

For results in same experiment (see [5]), for n=5 and for DC bias 95V, we have overall capacity change 100.97. This means that between neighboring vertices in graph we have capacity change $\frac{\Delta C}{C}$ of

$$\frac{\Delta C}{C} = 100.97/(n-1) = 100.97/4 = 25.2425$$

Appropriate neighboring matrix of this graph (for n=5) is

$$A = \begin{bmatrix} 0 & 25.2425 & 0 & 0 & 0 \\ 25.2425 & 0 & 25.2425 & 0 & 0 \\ 0 & 25.2425 & 0 & 25.2425 & 0 \\ 0 & 0 & 25.2425 & 0 & 25.2425 \\ 0 & 0 & 0 & 25.2425 & 0 \end{bmatrix}$$

In that case, we have parallel connection of capacity changes, and overall capacity change is equal to 100.97 (see [5]).

Let us make graph from one of 2D cases, for example with n=8 graines (see [5], see Fig.5). So, we have graph with same number of vertices (n=8),

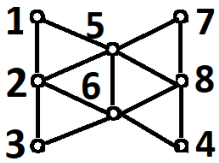

Fig. 5. Modelling with 2D graphs

If we use experimental results from [5] and if we divide overall capacitance change to local measure that characterizes relation between two grains (two vertices in graph). For example, for DC bias of 25V, we have overall capacity change of 69.45. This means that for *n=8, m=13* and for between neighboring vertices in graph we have capacity change $\frac{\Delta C}{C}$ of

$$\frac{\Delta C}{C} = 69.45/(n-1) = 69.45/12 = 5.7875$$

Appropriate neighboring matrix of this graph (see [10]) is

$$A = \begin{bmatrix} 0 & 5.7875 & 0 & 0 & 5.7875 & 0 & 0 & 0 \\ 5.7875 & 0 & 5.7875 & 0 & 5.7875 & 5.7875 & 0 & 0 \\ 0 & 5.7875 & 0 & 0 & 0 & 5.7875 & 0 & 0 \\ 0 & 0 & 0 & 0 & 0 & 5.7875 & 0 & 5.7875 \\ 5.7875 & 5.7875 & 0 & 0 & 0 & 5.7875 & 5.7875 & 5.7875 \\ 0 & 5.7875 & 5.7875 & 5.7875 & 5.7875 & 0 & 0 & 5.7875 \\ 0 & 0 & 0 & 0 & 5.7875 & 0 & 5.7875 & 0 \\ 0 & 0 & 0 & 5.7875 & 5.7875 & 5.7875 & 5.7875 & 0 \end{bmatrix}$$

This results to overall capacitance change equal to 68.73.

B. Modelling with 3D graphs

We will now apply 3D graphs on calculation of breakdown voltage on $BaTiO_3$ sample (see [1]) with some predefined constraints. Relation between grains in sample is established and described and now we have mathematical approach for calculation of breakdown voltage using experimental results. As a result, we introduced mapping between property of sample and grain structure, then between grain structure and mathematical graph, using various crystal structures. The main idea was to apply 3D-graph theory for distribution of electronic parameters between the neighboring grains. We will use simple $BaTiO_3$ sample, shown on Fig.6.

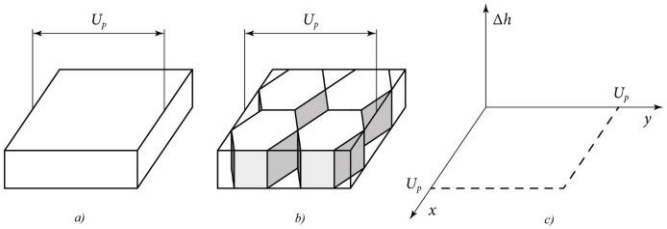

Fig. 6. $BaTiO_3$ sample with 4 grains.

Breakdown voltage U_p is obtained by measuring on whole sample, i.e.it is measured on two opposite sides of this sample. It is same in both directions, along x-axis and along y-axis (Fig. 2). Third dimension will be denoted with Δh, and that is vertical size of this sample, distance between top and bottom of the sample (tom and bottom of the grain).

If we do mapping of this grain sample (see [1]), onto 3D graph with eight vertices, shown on Fig.7. We put vertices on the top of each grain and at the bottom of each grain, assuming that there is also some value of U_p between grain ends. Breakdown voltage is very small and it can be neglected, leaving $U_p = \delta$, ($\delta \approx 0$). Assume that "dimensions" of this problem are now $x = 2$, $y = 2$ and $\Delta h = 2$.

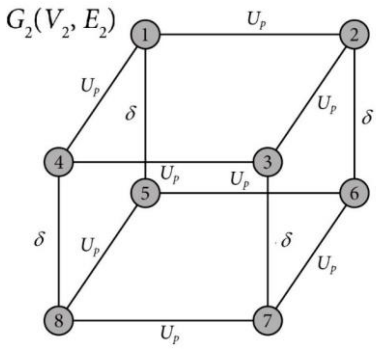

Fig. 7. 3D graph model of 2x2 grain sample, with 8 vertices.

Graph $G_2 = (V_2, E_2)$, has 8 vertices and 12 edges. Corresponding weight matrix of this graph is:

$$W_2 = \begin{bmatrix} 0 & U_p & 0 & U_p & \delta & 0 & 0 & 0 \\ U_p & 0 & U_p & 0 & 0 & \delta & 0 & 0 \\ 0 & U_p & 0 & U_p & 0 & 0 & \delta & 0 \\ U_p & 0 & U_p & 0 & 0 & 0 & 0 & \delta \\ \delta & 0 & 0 & 0 & 0 & U_p & 0 & U_p \\ 0 & \delta & 0 & 0 & U_p & 0 & U_p & 0 \\ 0 & 0 & \delta & 0 & 0 & U_p & 0 & U_p \\ 0 & 0 & 0 & \delta & U_p & 0 & U_p & 0 \end{bmatrix}$$

Each "horizontal" (along x-axis and along y-axis) edge of this graph has the same weight U_p, and each "vertical" edge (between top and bottom of the grain) has the same weight δ. In the case obtained from the experiment in [1], case I-16 $BaTiO_3$ ceramics without additives, we have:

$$W_2 = \begin{bmatrix} 0 & 12.54 & 0 & 12.54 & \delta & 0 & 0 & 0 \\ 12.54 & 0 & 12.54 & 0 & 0 & \delta & 0 & 0 \\ 0 & 12.54 & 0 & 12.54 & 0 & 0 & \delta & 0 \\ 12.54 & 0 & 12.54 & 0 & 0 & 0 & 0 & \delta \\ \delta & 0 & 0 & 0 & 0 & 12.54 & 0 & 12.54 \\ 0 & \delta & 0 & 0 & 12.54 & 0 & 12.54 & 0 \\ 0 & 0 & \delta & 0 & 0 & 12.54 & 0 & 12.54 \\ 0 & 0 & 0 & \delta & 12.54 & 0 & 12.54 & 0 \end{bmatrix}, (\delta \approx 0).$$

After that, we do the mapping of the same grain sample onto 3D graph with nine vertices, shown on next Fig.8. We put vertices on "top" of each grain and also on "bottom" of each grain (see [1]), like in previous case, breakdown voltage between those ends is very small, so we will assume that it is δ. New, ninth vertex is, by BCC principle (body-centered cubic crystal system imaginary point in the middle of this sample, and its appearance rises gives dimension of this problem from 2 to 3. Assume that "dimensions" of problem are $x = 2, y = 2$ and $\Delta h = 3$.

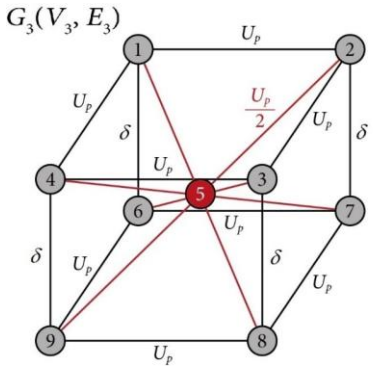

Fig. 8. 3D graph model (Body-centered in crystal system) with 9 vertices.

Graph $G_3 = (V_3, E_3)$, has a set of 9 vertices and a set of 20 edges (see [1]). Corresponding weight matrix of this graph is:

$$W_3 = \begin{bmatrix} 0 & U_p & 0 & U_p & U_p/2 & \delta & 0 & 0 & 0 \\ U_p & 0 & U_p & 0 & U_p/2 & 0 & \delta & 0 & 0 \\ 0 & U_p & 0 & U_p & U_p/2 & 0 & 0 & \delta & 0 \\ U_p & 0 & U_p & 0 & U_p/2 & 0 & 0 & 0 & \delta \\ U_p/2 & U_p/2 & U_p/2 & U_p/2 & U_p/2 & U_p/2 & U_p/2 & U_p/2 & U_p/2 \\ \delta & 0 & 0 & 0 & U_p/2 & U_p & 0 & U_p & 0 \\ 0 & \delta & 0 & 0 & U_p/2 & 0 & U_p & 0 & U_p \\ 0 & 0 & \delta & 0 & U_p/2 & U_p & 0 & U_p & 0 \\ 0 & 0 & 0 & \delta & U_p/2 & 0 & U_p & 0 & U_p \end{bmatrix}$$

Each "horizontal" edge of this graph has the same weight U_p, and each "vertical" edge, that goes "through" the grain have same weight δ. In case obtained from the experiment (see [1]), we have:

$$W_3 = \begin{bmatrix} 0 & 12.54 & 0 & 12.54 & 6.27 & \delta & 0 & 0 & 0 \\ 12.54 & 0 & 12.54 & 0 & 6.27 & 0 & \delta & 0 & 0 \\ 0 & 12.54 & 0 & 12.54 & 6.27 & 0 & 0 & \delta & 0 \\ 12.54 & 0 & 12.54 & 0 & 6.27 & 0 & 0 & 0 & \delta \\ 6.27 & 6.27 & 6.27 & 6.27 & 6.27 & 6.27 & 6.27 & 6.27 & 6.27 \\ \delta & 0 & 0 & 0 & 6.27 & 12.54 & 0 & 12.54 & 0 \\ 0 & \delta & 0 & 0 & 6.27 & 0 & 12.54 & 0 & 12.54 \\ 0 & 0 & \delta & 0 & 6.27 & 12.54 & 0 & 12.54 & 0 \\ 0 & 0 & 0 & \delta & 6.27 & 0 & 12.54 & 0 & 12.54 \end{bmatrix}, (\delta \approx 0).$$

Now, we can discuss same grain sample, mapped onto 3D graph, but now with twelve vertices, shown on Fig.9. New imaginary vertices are pointed in the middle of each surface of this sample, except upper surface and bottom surface. "Dimensions" of problem are $x = 2, y = 2$ and $\Delta h = 3$.

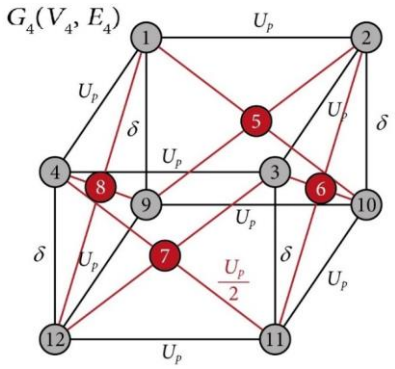

Fig. 9. 3D graph model (Face-centered in crystal system) with 12 vertices.

Corresponding weight matrix (see [1]) of this graph is

$$W_4 = \begin{bmatrix}
0 & U_p & 0 & U_p & U_p/2 & 0 & 0 & U_p/2 & \delta & 0 & 0 & 0 \\
U_p & 0 & U_p & 0 & U_p/2 & U_p/2 & 0 & 0 & 0 & \delta & 0 & 0 \\
0 & U_p & 0 & U_p & 0 & U_p/2 & U_p/2 & 0 & 0 & 0 & \delta & 0 \\
U_p & 0 & U_p & 0 & 0 & 0 & U_p/2 & U_p/2 & 0 & 0 & 0 & \delta \\
U_p/2 & U_p/2 & 0 & 0 & 0 & 0 & 0 & 0 & U_p/2 & U_p/2 & 0 & 0 \\
0 & U_p/2 & U_p/2 & 0 & 0 & 0 & 0 & 0 & 0 & U_p/2 & U_p/2 & 0 \\
0 & 0 & U_p/2 & U_p/2 & 0 & 0 & 0 & 0 & 0 & 0 & U_p/2 & U_p/2 \\
U_p/2 & 0 & 0 & U_p/2 & 0 & 0 & 0 & 0 & U_p/2 & 0 & 0 & U_p/2 \\
\delta & 0 & 0 & 0 & U_p/2 & 0 & 0 & U_p/2 & 0 & U_p & 0 & U_p \\
0 & \delta & 0 & 0 & U_p/2 & U_p/2 & 0 & 0 & U_p & 0 & U_p & 0 \\
0 & 0 & \delta & 0 & 0 & U_p/2 & U_p/2 & 0 & 0 & U_p & 0 & U_p \\
0 & 0 & 0 & \delta & 0 & 0 & U_p/2 & U_p/2 & U_p & 0 & U_p & 0
\end{bmatrix}$$

Each "horizontal" edge of this graph has same weight U_p, and each "vertical" edge, that goes "through" the grain have same weight δ. For $BaTiO_3$ ceramics (see [1]) without additives, we have:

$$W_4 = \begin{bmatrix}
0 & 12.54 & 0 & 12.54 & 6.27 & 0 & 0 & 6.27 & \delta & 0 & 0 & 0 \\
12.54 & 0 & 12.54 & 0 & 6.27 & 6.27 & 0 & 0 & 0 & \delta & 0 & 0 \\
0 & 12.54 & 0 & 12.54 & 0 & 6.27 & 6.27 & 0 & 0 & 0 & \delta & 0 \\
12.54 & 0 & 12.54 & 0 & 0 & 0 & 6.27 & 6.27 & 0 & 0 & 0 & \delta \\
6.27 & 6.27 & 0 & 0 & 0 & 0 & 0 & 0 & 6.27 & 6.27 & 0 & 0 \\
0 & 6.27 & 6.27 & 0 & 0 & 0 & 0 & 0 & 0 & 6.27 & 6.27 & 0 \\
0 & 0 & 6.27 & 6.27 & 0 & 0 & 0 & 0 & 0 & 0 & 6.27 & 6.27 \\
6.27 & 0 & 0 & 6.27 & 0 & 0 & 0 & 0 & 6.27 & 0 & 0 & 6.27 \\
\delta & 0 & 0 & 0 & 6.27 & 0 & 0 & 6.27 & 0 & 12.54 & 0 & 12.54 \\
0 & \delta & 0 & 0 & 6.27 & 6.27 & 0 & 0 & 12.54 & 0 & 12.54 & 0 \\
0 & 0 & \delta & 0 & 0 & 6.27 & 6.27 & 0 & 0 & 12.54 & 0 & 12.54 \\
0 & 0 & 0 & \delta & 0 & 0 & 6.27 & 6.27 & 12.54 & 0 & 12.54 & 0
\end{bmatrix},$$

where $\delta \approx 0$.

III. SINTETIZED DIAMONDS AS BIOMIMETIC MATERIALS

Materials science is spreading into all fields of basic and applied science. One of the biggest influence on everydays life in bioceramics materials is the application of these substrates for medical engineering (see [4]). The most prominent bio-relevant properties of a biomaterial are chemical inertness and bio-durability, so submicro diamond is coming into the center of our research interest. This diamond structure is an unique biomaterial with specific compatible characteristics, which are not exactly only one based on its bio-chemical properties. Physical-chemical biocompatibility directions, including data from nano interface water layers could be defined on nanodiamond substrates (see [4]). If we, theoretical, split diamond surface into small particles, we can implement similar approach like with grains in [5]. If we take a small part of diamond surface, of "dimension" 2x2x1 (Fig.6), we can detect and assign graph vertices in upper surface of diamond, shown on Fig.10.

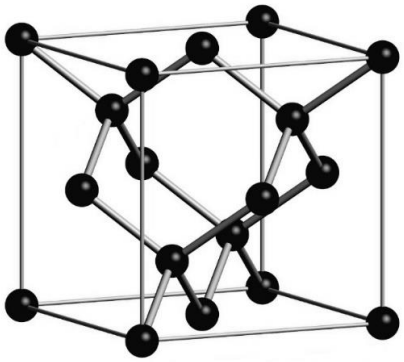

Fig. 10. Syntetized diamond internal structure.

Appropriate graph is shown on Fig.11. We can assume some property (any electrical, dielectrical or magnetic property), noted with v, and we can assign values on those graph edges, we can represent this graph (see [4]) with weight matrix W.

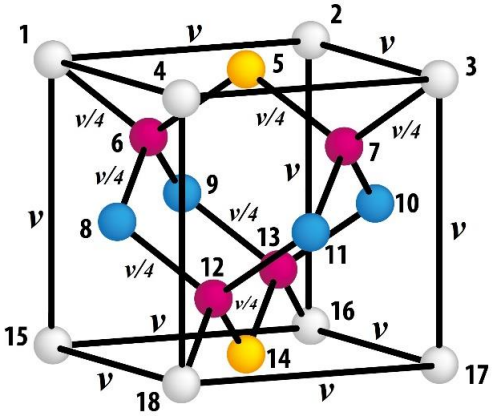

Fig. 11. 3D graph model of syntetized diamond

Weight matrix of this graph (see [4]) is:

$$W = \begin{bmatrix}
0 & v & 0 & v & 0 & v/4 & 0 & 0 & 0 & 0 & 0 & 0 & 0 & v & 0 & 0 & 0 \\
v & 0 & v & 0 & 0 & 0 & 0 & 0 & 0 & 0 & 0 & 0 & 0 & 0 & v & 0 & 0 \\
0 & v & 0 & v & 0 & 0 & v/4 & 0 & 0 & 0 & 0 & 0 & 0 & 0 & 0 & v & 0 \\
v & 0 & v & 0 & 0 & 0 & 0 & 0 & 0 & 0 & 0 & 0 & 0 & 0 & 0 & 0 & v \\
0 & 0 & 0 & 0 & 0 & v/4 & v/4 & 0 & 0 & 0 & 0 & 0 & 0 & 0 & 0 & 0 & 0 \\
v/4 & 0 & 0 & 0 & v/4 & 0 & 0 & v/4 & v/4 & 0 & 0 & 0 & 0 & 0 & 0 & 0 & 0 \\
0 & 0 & v/4 & 0 & v/4 & 0 & 0 & 0 & 0 & v/4 & v/4 & 0 & 0 & 0 & 0 & 0 & 0 \\
0 & 0 & 0 & 0 & 0 & v/4 & 0 & 0 & 0 & 0 & 0 & v/4 & 0 & 0 & 0 & 0 & 0 \\
0 & 0 & 0 & 0 & 0 & v/4 & 0 & 0 & 0 & 0 & 0 & 0 & v/4 & 0 & 0 & 0 & 0 \\
0 & 0 & 0 & 0 & 0 & 0 & v/4 & 0 & 0 & 0 & 0 & 0 & v/4 & 0 & 0 & 0 & 0 \\
0 & 0 & 0 & 0 & 0 & 0 & 0 & v/4 & 0 & 0 & 0 & 0 & 0 & v/4 & 0 & 0 & 0 \\
0 & 0 & 0 & 0 & 0 & 0 & 0 & 0 & v/4 & 0 & 0 & v/4 & 0 & 0 & v/4 & 0 & 0 \\
0 & 0 & 0 & 0 & 0 & 0 & 0 & 0 & 0 & v/4 & v/4 & 0 & 0 & 0 & v/4 & v/4 & 0 \\
0 & 0 & 0 & 0 & 0 & 0 & 0 & 0 & 0 & 0 & 0 & v/4 & v/4 & 0 & 0 & 0 & 0 \\
v & 0 & 0 & 0 & 0 & 0 & 0 & 0 & 0 & 0 & 0 & 0 & 0 & 0 & v & 0 & v \\
0 & v & 0 & 0 & 0 & 0 & 0 & 0 & 0 & 0 & 0 & v/4 & 0 & v & 0 & v & 0 \\
0 & 0 & v & 0 & 0 & 0 & 0 & 0 & 0 & 0 & 0 & 0 & 0 & v & 0 & v & 0 \\
0 & 0 & 0 & v & 0 & 0 & 0 & 0 & 0 & 0 & 0 & v/4 & 0 & 0 & v & 0 & v
\end{bmatrix}$$

Each "horizontal" edge of this graph has weight v, direct "vertical" edge also has weight v, and "skew" edges, through structure has weight $v/4$. Why divided with 4? Because in this model every algebraic path through this graph, starting from upper surface down to lower surface, consist of 4 edges, length of algebraic path is 4 (see [4]).

The ultra-nanocrystalline synthetized diamonds are very advanced materials for biomedical and other applications. We pointed out to a complex relation between graph theory and electrophysical parameters of the consolidated nano-diamonds is presented. We performed and explained related experimental procedure with results data (see [4]). By this method we provided way for defining the electrophysical parameters on micro and nano level of grains and pores, what is important for further designing microelectronic structures and advance miniaturization.

IV. Outlook

In the future research, it is possible to correlate graph theory application on some other ceramic materials characteristics and to use it for some other values calculation on microlevel, for example electrical conductivity, thermal conductivity, etc. Also, it could be very important to compare the results based on neural networks and graph application, simultaneously. The nanocrystalline synthetized diamonds are very advanced materials for high-tech applications especially in medicine, electronic and space research. Further application of the graph theory decelopment could make some new and unexpected contributions in this field.

V. Conclusion

In this research paper we intended to make an overview on a complex relation between graph theory, BaTiO3-ceramics and synthetized diamonds electrophysical parameters calculations, and also designed microeletronic intergranular relations. Before the graph and neural network theories (see [10-14]), we have used different experimental methods for global measurements and collecting the physical parameters from the sample surfaces, based mostly on the statistic distribution.

Now we can define values directly at the level of the grains and pores, and, also, between them. Based on this approacch we provided a way for defining other parameters on micro and nano grains and pores constituents, what is important for advance predicting microelectronic structures and related parameters, in electronic material sciences in general.

References

[1] V.V.Mitic, B.Randjelovic, I.Ilic, S.Ribar, **C**.An-Lu, A.Stajcic, B.Vlahovic."The 3D graph approach for breakdown voltage calculation in BaTiO3 ceramics", IJMPB, Vol 35 (7) (2021) pp. 2150103.

[2] V.V.Mitic, G.Lazovic, B.Randjelovic, V.Paunovic, I.Radovic, A.Stajcic, B.Vlahovic: "Graph Theory Applied to Microelectronic Intergranular Relations", Ferroelectrics, 570 (2021) p. 145-152.

[3] V. Mitić, C.A.Lu, B.Randjelović, V. Paunović, I.Radovic, A. Stajcic, J.Kotnik, H.Fecht, B. Vlahovic, "3D graph theory application on modified nano BaTiO3 electronic ceramics", Int.Conf. Electronic Materials and Applications EMA-2021, Virtual, January 19-21, 2021.

[4] B.Ranđelović, V.V.Mitic, S.Ribar, M.Cebela, M.Mohr, H.Fecht, B.Vlahovic: "Graph Theory Approach in Synthetized Diamond Electrophysical Parameters Defining", in: Bioceramics, Biomimetic and other Compatible Materials Features for Medical Applications (Ed: S.Najman., V.V.Mitic, T.Groth, M.Barbeck, P.Yu Chen, Z.Sun), Springer Nature, Cham, Switzerland, 2021, accepted.

[5] B.Randjelovic, V.V.Mitic, S.Ribar, I.Radovic, A.Stajcic, I.Novakovic, B.Vlahovic. "Ceramics, Materials, Microelectronics and Graph Theory new Frontiers", MPLB, Vol 34 (34) (2020) pp.2150159.

[6] V. Mitlić, G. Lazović, B.M. Randjelović, V. Paunović, J.M. Wu D.Mancić,, J.R. Hwu, "Fractal Microeletronic Frontiers and Graph Theory Applications", Int.Conference MS&T **2019**, Book of Abstracts, Portland, USA, 29 September – 03 October 2019.

[7] V. Mitić, G. Lazović, C.A.Lu, I.Radovic, V. Paunović, A. Stajcic, B.Randjelović, S.Ribar, B. Vlahovic, "Investigation of intergranular dielectric properties within the relation between fractal, graph and neural networks theories", Int.Conf. Electronic Materials and Applications EMA-2021, Virtual, January 19-21, 2021.

[8] V. Mitić, C. Serpa, C.A.Lu, V. Paunović, I.Radovic, B.Randjelović, S.Ribar, A. Stajcic, B. Vlahovic, "Fractal, graph and neural network theories applied on BaTiO3 electronic ceramics", Int.Conf. Electronic Materials and Applications EMA-2021, Virtual, January 19-21, 2021.

[9] V. Mitić, I.Radovic, C.A.Lu, S.Ribar, B.Randjelović, A. Stajcic, H. Fecht, B. Vlahovic, "Neural networks and applied graph theory approaches for intergranular properties measurements investigation", Int.Conf. Electronic Materials and Applications EMA-2021, Virtual, January 19-21, 2021.

[10] Mitic V. V.. *et al*. The Artificial Neural Networks Applied for Microelectronics Intergranular 323 Relations Determination. *Integrated Ferroelectics*. 212 .(2020).

[11] V.V.Mitic, S.Ribar, B.Randjelovic, C.-A. Lu, I.Radovic, A.Stajcic, I.Novakovic, B.Vlahovic, Neural Networks and Microelectronic Parameters Distribution Measurements depending on Sinthering Temperature and Applied Voltage, MPL B, 34 (**35)** (2020) pp. 2150172.

[12] Mitic V. V *et al.* Sinterign Temperature Influenceo on Grains Function Distribution by Neural Network Application, Thermal Science (2021) (accepted).

[13] Ribar S. *et al.* Neural Networks from Biophysical Applications in Microelectronics Parameters 336 Measurements. in: *Bioceramics. Biomimetic and other Compatible Materials Features for* 337 *Medical Applications.* (Ed. Najman S.. Mitic V.. Groth T.. Barbeck M.. Yu Chen P.. Sun Z.). 338 Springer Nature. Cham. Switzerland. 2021. accepted for publication

[14] Ribar S. *et al*. Neural Networks Application on Human Skin Biophysical Impedance 319 Characterisations. *Biophysical Reviews & Letters*. 16.(2021). pp. 2021 – 19

Biomolecules and Brownian Motion

Vojislav V. Mitić, Bojana Marković, Sanja Aleksić, Dušan Milošević, Branislav Randjelović, Ivana Ilić, Jelena Manojlović and Branislav Vlahović

***Abstract*—Structures and different life functions of microorganisms, like motion, are based on molecular biology processes, which comprise molecular and submolecular particles. It is very important to determine relation between molecular and microorganisms levels. The aim of our research is the analysis of Brownian motion as a general phenomenon and the consequence of structures hierarchy from molecular to microorganisms level. If we approach this idea from the aspect of biomimetic correlations at the level of the alive and nonalive matter system particles, the condensed matter particles could be considered as a part of micro, nano and molecular microorganisms structures. In this research we used the experimental results of bacterial motion influenced by different energy impulses. The important goal of this research paper is to obtain significant data regarding Brownian motion in the frame of fractal nature similarities, as an integrative property of living and nonliving systems particles processes. This opens new frontiers for submicroelectronics relations within the integrated supermicro biophysical systems. This is a potential new trend in nowadays advanced research, where we integrate the knowledges of complex relations between the electrons or other particles and their clusters as joint structures in alive and condensed matter, what could be a possible direction for new microelectronics complex biodevices and integrations.**

***Index Terms*—molecular biology; microorganisms; Brownian motion; biomimetic; fractals.**

Vojislav V. Mitić is with the Faculty of Electronic Engineering, University of Nis, 14 Aleksandra Medvedeva, 18000 Nis, Serbia and Institute of Technical Sciences of SASA, 35 Kneza Mihaila, 11000 Belgrade, Serbia (e-mail: vmitic.d2480@gmail.com).

Bojana Marković is with the Faculty of Electronic Engineering, University of Nis, 14 Aleksandra Medvedeva, 18000 Nis, Serbia (e-mail: bojana.markovic123@gmail.com).

Sanja Aleksić is with the Faculty of Electronic Engineering, University of Nis, 14 Aleksandra Medvedeva, 18000 Nis, Serbia (e-mail: sanja.aleksic@elfak.ni.ac.rs).

Dušan Milošević is with the Faculty of Electronic Engineering, University of Nis, 14 Aleksandra Medvedeva, 18000 Nis, Serbia (e-mail: dusan.milosevic@elfak.ni.ac.rs).

Branislav Randjelović is with the Faculty of Electronic Engineering, University of Nis, 14 Aleksandra Medvedeva, 18000 Nis, Serbia and Faculty of Teachers Educationin Prizren - Leposavić, University of Priština - Kosovska Mitrovica, Nemanjina, 38218 Leposavić, Serbia (e-mail: branislav.randjelovic@elfak.ni.ac.rs).

Ivana Ilić is with the Medical Faculty, Department for Mathematics and Informatics, University of Nis, 81 Bul. Dr Zorana Djindjića, 18000 Nis, Serbia (e-mail: ivanailicc3@gmail.com).

Jelena Manojlović is with the Faculty of Mechanical Engineering, University of Nis, 14 Aleksandra Medvedeva, 18000 Nis, Serbia (e-mail: jmanojlo@gmail.com).

Branislav Vlahović is with the North Carolina Central University, USA Durham NC, USA (e-mail: vlahovic@nccu.edu).

I. Introduction

Phenomena that exist in both living and nonliving matter, as electron and molecular motion, are to be considered from different aspects and they require a multidisciplinary approach. Molecular biology, as a life science, studies various processes in alive organisms at the molecular level. Thus, electron motion in biomolecules as well as molecular motion, belong within the molecular biology and molecular bioelectronics research field.

Electron motion is based on the same principles in alive organisms and in condensed matter, so it should be observed as a joint property to get the complete insight into this fundamental process. Based on our current knowledge and possibilities, we are not able to determine electron motion. However, we can determine motion of the molecules that contain those electrons. Every molecule which is moving, carries an electron cluster making it move as well. Within molecules as parts of biosystems, existing atoms and electrons „are not aware of“ whether they are a part of an alive organism or condensed matter. That is very important because it distinguishes the molecule as the significant integrative factor between living and nonliving systems.

The idea of biomimetic correlation between molecular and submolecular particles of alive and nonalive matter, in the frame of the Brownian motion fractal nature characterization, implies the entire new possibility of considering these particles motion as the biunivocal phenomenon. Microorganisms and viruses demonstrate biomimetic similarities with condensed matter particles motion because of their dimensions and motion patterns [1]. Bacteria motility behavior, which implies velocity, direction and trajectory, is also influenced by environmental changes like temperature, pH, or different energetic impulses [2].

We used Brownian motion fractal nature, as a general characteristic of both alive and nonalive systems, to establish the relation between these two different systems, but consisting of identical particles. Also, we plan to develop the biophysical-mathematical asymptotic approaching model for living organisms and condensed matter particles, as they are biunivocaly correspondent.

One of the objectives of our research is to explain the Brownian motion as the joint characteristic of biomolecule and physical system particles. Controling particles motion and predicting their trajectories [3] in this kind of biomimetic approach [4], provides new perspectives for

further microelectronics miniaturization and electronics parameter integrations [5,6].

So, our goal is to characterize the molecular motion based on Brownian motion within the combination of the experimental and the theoretical experiment results.

II. EXPERIMENTAL METHODS AND PROCEDURES

We performed real experiments with diverse bacteria in a liquid phase under the influence of variant energy impulses [7], among which were some different music impulses (Figure 1). In that sense, we got some data from which we generated the two and three dimensional diagrams [2,7].

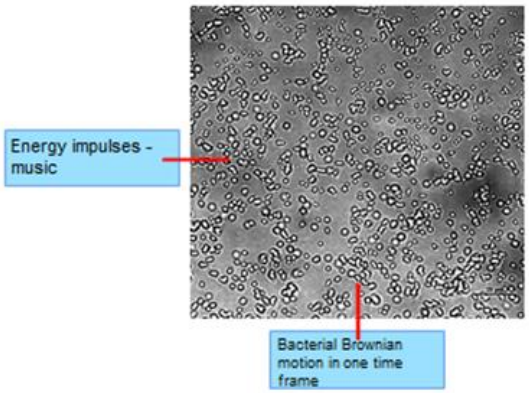

Fig. 1. The bacterial motion experiment diagram.

Now, our intension is to generate the analytical forms. Also, we used some other available research results which are based on molecular motions [8]. In this case we treat the molecules like clusters of electrones in different matter organizations from atomic to molecular level. This way we avoid the lack of worldwide research recorded electron motions. Hence, we now observe the molecules as "packages" of electrons or other particles. From the other hand, we also analyze all of these molecules as a part of alive bacterial matter. At the end, we can jointly understand the biophysical integrated systems with one important characteristic and that is just the Brownian motion.

A. *Mathematical Background*

It is well known that it is possible to create some mathematical model describing the relationship between several quantities. By using one of them, called the dependent variable (we will denote it by y) and one or more quantities, called the independent variables (we will denote them by $x_1, x_2 \dots x_n$,), we can obtain a model which represents a linear relationship between the dependent variable and independent variables in the form:

$$y = a_1x_1 + a_2x_2 + \cdots + a_nx_n + b, \quad (1)$$

where $a_1, a_2 \dots a_n$, b are real (or complex) numbers. If the value of the variable y depends only on one independent variable x, then (1) has a form:

$$y = ax + b. \quad (2)$$

This formula could be obtained by applying various numerical approximation models. One of very useful approximation models is the least square approximation.

The least squares method (also called discrete mean square approximation [9]) belongs to the so-called best approximations, i.e. approximation methods in which the criterion is the minimization of the error according to one of the norms. Specifically, this is the norm L^2, ie. the total sum of the squares of the errors in the approximation nodes is minimized [9,10]. Some of the interesting applications of those methods are already given in [11-13].

B. *Main Results*

We applied the technique to the data in Table I, which describes the coordinates of bacteria locations, during movement through coordinate system [7].

TABLE I
BACTERIA LOCATIONS COORDINATES

i	x_i	y_i	z_i
1	0	0	0
2	0.1043	-0.3698	-0.2869
3	0.0521	-0.4622	-0.3641
4	0.0521	-0.2773	-0.4809
5	0.0521	-0.2773	-0.7842
6	0.0521	-0.1849	-0.7605
7	0.1564	-0.5547	-0.7709
8	0.2607	-0.7396	-0.7757
9	0.5213	-0.7396	-1.0163
10	0.4170	-0.8320	-0.9330
11	0.3649	-0.8320	-0.9349

Based on the data from Table I, we obtained the 3D diagram presented in Figure 2.

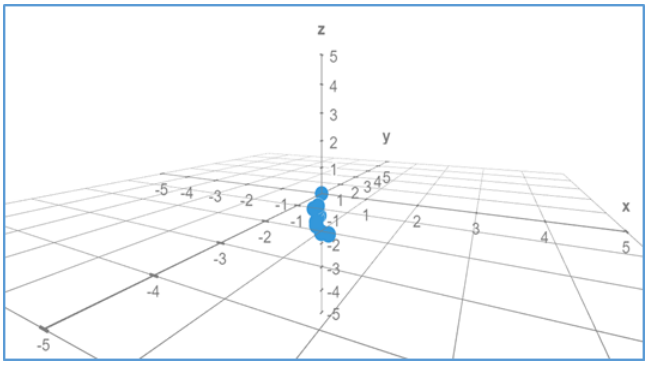

Fig. 2. The points of the bacteria locations in 3D.

Next, we considered four molecule location points in 3D given in Table II and presented in Figure 3.

TABLE II
MOLECULE LOCATIONS COORDINATES

i	x_i	y_i	z_i

1	2	5.8	4
2	2.2	2	4.2
3	2.5	4.4	4.5
4	2.8	3.2	5.2

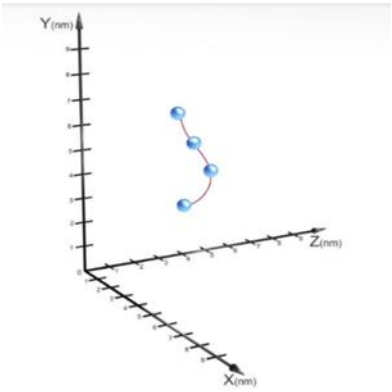

Fig. 3. 3D diagram of molecule motion in different time intervals.

III. RESULTS AND DISCUSSION

We applied multiple linear regression, to determine the mutual dependence of the coordinates and to obtain explicit formula for predicting and calculating positions.

Based on the data from Table I, we will apply the procedure of forming an approximation function

$$\varphi(x, y) = ax + by + c, \tag{3}$$

by using the least squares method. Thus, by applying the least square approximation (the operational software was statistical package in Excel) on the given data sets, we obtained next results considering the best linear fit for the presented model: the coefficients of the resulting linear function are respectfully a=–1,47999912, b=–0,02844679 and c=–0,36733904 and the estimated regression function is of the form:

$$\varphi(x, y) = -0.746871x - 0.421536y - 0.306160 \tag{4}$$

We can compare values and precision of dependent variables $\boldsymbol{z_i}$ in given points and results obtained by formula trough the absolute and relative error (Table 3).

TABLE III
COMPARISON BETWEEN REAL AND APPROXIMATE COORDINATES, ABSOLUTE AND RELATIVE ERROR

x_i	y_i	z_i	φ_i	Δ	%
0	0	0	-0.3061600	0.3061600	
0.1043	-0.3698	-0.2869	-0.5399426	0.2530427	-88.20%
0.0521	-0.4622	-0.3641	-0.5399059	0.1758059	-48.29%
0.0521	-0.2773	-0.4809	-0.4619639	0.0189361	-3.94%
0.0521	-0.2773	-0.7842	-0.4619639	0.3222361	-41.09%
0.0521	-0.1849	-0.7605	-0.4230139	0.3374860	-44.38%
0.1564	-0.5547	-0.7709	-0.6567966	0.1141034	-14.80%
0.2607	-0.7396	-0.7757	-0.8126373	0.0369373	-4.76%
0.5213	-0.7396	-1.0163	-1.0072718	0.0090281	-0.89%
0.4170	-0.8320	-0.9330	-0.9683232	0.0353232	-3.79%
0.3649	-0.8320	-0.9349	-0.9294112	0.0054888	-0.59%

The plot (4) obtained with the least squares method is presented in Figure 4.

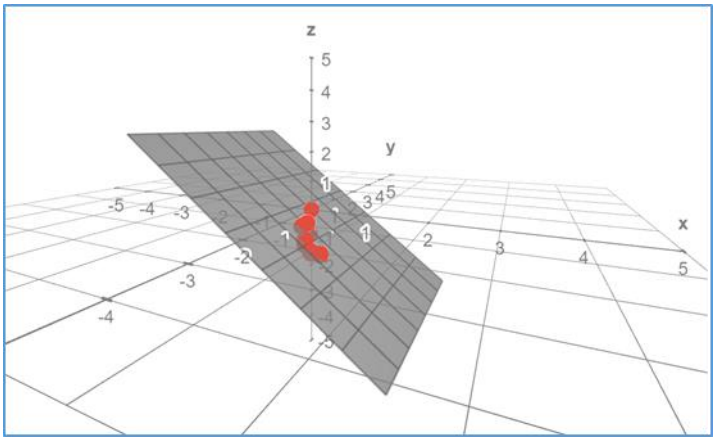

Fig. 4. The approximation plot with marked red points from Table III.

Similarly, as in previous procedure applied on bacterial motion experimental data, we obtained next results for molecule motion in different time intervals, considering the best linear fit for the presented model: the coefficients of the resulting linear function are respectfully a=1.4685067, b=0.0035386 and c=0.973673 and the estimated regression function is of the form:

$$\varphi = 1.4685067x + 0.0035386y + 0.973673. \tag{5}$$

Next, by using the estimated regression function (5) and by implementing the 2D coordinates we obtained the estimated dependent values of the z-coordinates, presented in the Table IV, together with the evaluated absolute and relative error of this approximation:

TABLE IV
Z- COORDINATES WITH THE ABSOLUTE AND RELATIVE ERROR

x_i	y_i	z_i	φ_i	Δ	%
0	0	0			
2	5.8	4	3.9312102	0.0687898	1.72%
2.2	2	4.2	4.2114649	0.0114649	0.27%
2.5	4.4	4.5	4.6605095	0.1605096	3.57%
2.8	3.2	5.2	5.0968150	0.1031850	1.98%

The plot (5) obtained with the least squares method is presented in Figure 5.

If we observe alive and nonalive matter particles as a hierarchical phenomenon, we can consider an atom as a

cluster of electrons and other particles, a molecule as a cluster of atoms with already mentioned particles which are penetrating each other from their orbitals in interatomic relations within the molecule, and a microorganism as a cluster of molecules. Nowadays fundamental research and science do not have high-tech and also resolution possibilities to recognize, separately, the electron motion. We can consider only the indirect effects. Here, we must stress the complexity in the matter based on quantum mechanical principles and Heisenberg uncertainty principle, as well, in all of these considerations.

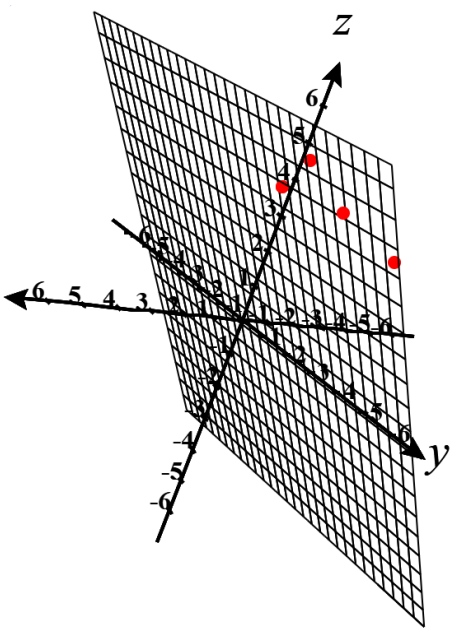

Fig. 5. The approximation plot with marked red points from Table IV.

Each bacterial cell comprises 2 – 4 millions of protein molecules [14], which implies that the total number of molecules per bacterial cell is much higher. This is just one comparison. We can observe the effect of electron motion at the molecular and microorganisms level. So definitely, the particles motion based on Brownian motion fractals effects, is the base for deeply understanding all of these processes within the submicro scale sizes with the joint characteristic which we can nominate as "actio in distans" in motion.

In this paper we introduced two mathematical analytical forms: one for bacterial and second for molecular motion, which are characterized by Brownian motion. In that sense we would like to establish a relation between these two mathematical analytical forms considering molecule number ratio. In this way we could determine asymptotic approaching of two mathematical functions towards fractals biomimetical self-similarity. This is the idea for our further research.

IV. OUTLOOK

All of these results and innovative methods in mathematical analysis and discussions are just the original start in this field. In the next step we plan to develop a method by which we can establish the relation between the analytical mathematics and asymptotic approaching of alive and nonalive matter particles, with an idea to do it by fractal similarities.

V. CONCLUSION

In this paper we performed the results regarding molecular and bacterial motion. Regarding molecular motion, comprising electron motion, we provided mathematical analytical forms, in order to substantially characterize this motion. We analyzed bacterial motion influenced by different energy impulses, like music, and presented obtained data, showing random bacterial trajectories based on Brownian motion, in mathematical analytical forms, as well. Thus, in this stage we fulfilled and satisfied the idea of "electron clusters" in biomolecules which are also a part of microorganisms. Here, we define just a beginning of the joint integration in biophysical systems with general characteristic which is the Brownian motion.

ACKNOWLEDGMENT

The authors gratefully acknowledge the support of Ministry of Education, Science and Technological Development of Serbia, and The National Science Foundation of North Carolina, USA, for this research.

REFERENCES

[1] V.V.Mitic,G.Lazovic, D.Milosevic, E.Ristanovic, D.Simeunovic,S.-C. Tsay, M.Milosevic and B.Vlahovic, "Brownian fractal nature Coronavirus motion," *Mod. Phys. Lett. B*, vol. 35, no. 04, pp. 2150076, Jan. 2021.

[2] V.V. Mitic, G. Lazovic , D. Milosevic, C.-A. Lu, J. Manojlovic, S.-C. Tsay, S. Kruchinin and B. Vlahovic, "Brownian motion and fractal nature," *Mod. Phys. Lett. B*, vol.34, no. 19n20, pp. 1-11, July, 2020.

[3] Z. B. Vosika, V. V. Mitić, G. Lazović, V. Paunović and Lj. Kocić, "Meso-kinetics of one time relaxation electrical processes in BaTiO3 ceramics—modified Boltzmann-Poisson model," *Ferroelectrics*, vol. 531, pp. 38–50, Nov, 2018.

[4] J. Mei, X. Peng, Q. Zhang, X. Zhang, T. Liao, V.V. Mitic and Z, Sun, "Bamboo-membrane inspired multilevel ultrafast interlayer ion transport for superior volumetric energy storage," *Adv. Funct. Mater*, May, 2021.

[5] V.V. Mitic, S.Ribar, B.Randjelovic, C.-A. Lu, I. Radovic, A. Stajcic, I.Novakovic and B.Vlahovic, "Neural networks and microelectronics parameters distribution measurements depending on sintering temperature and applied voltage," *Mod. Phys. Lett. B*, vol.34, no. 35, pp. 2150172, Dec, 2020.

[6] V. V. Mitic, G. Lazovic, S. Ribar, C.-A. Lu, I. Radovic, A. Stajcic, H. Fecht and B. Vlahovic, "The artificial neural networks applied for microelectronics intergranular relations determination," *Integr. Ferroelectr*, vol. 212, pp. 135–146, Nov, 2020.

[7] V.V. Mitic, G. Lazovic, D. Milosevic, J. Manojlovic, E. Ristanovic, D. Simeunovic, S.-C. Tsay, M. Milosevic, M. Sokovic and B. Vlahovic, "Brownian motion fractal nature frontiers within the matter," in *Biocompatible and Biomimetic Features of Materials for*

Biomedical Applications – New Insights, Switzerland, Springer, 2021, ch. 10.

[8] S. Bhunia, A. Rana, P. Roy, D. J. Martin,M. L. Pegis, B. Roy and A. Dey, "Rational design of mononuclear iron-porphyrins for facile and selective 4e-/4H+ O2 reduction: activation of O-O bond by 2nd sphere hydrogen bonding," *J. Am. Chem. Soc,* vol. 140, no.30, pp. 9444-9457, July, 2018.

[9] G.V.Milovanović, *Numerical analysis II*, 3rd ed. Belgrade, Serbia, Naucna Knjiga,1991, VIII+210 pp.

[10] G.V.Milovanović and M.A.Kovačević, *A collection of solutions for problems in numerical analysis*, 3rd ed. Belgrade, Serbia, Naucna Knjiga,1991, IV+278 pp.

[11] B.Ranđelović, I.Radojković and B.Gajić, "One Application of Discrete Mean Squere Approximation For Prediction of Voluntary Pension Fund Development," *Appl. Math. and Comp. Science*, vol 5, no. 1, University of Nis, Faculty of Science, pp.7-15, 2020.

[12] I.D.Radojkovic**,** B.Gajic and B.M.Randjelovic, "Predicting the Development of Voluntary Pension Funds in Serbia by Applying The Mathematical Method of Linear Regression," *J. of Economic and Social Development – Resilient Society*, vol. 8, no. 1, pp. 2-13, 2021.

[13] I.D.Radojkovic, B.M.Randjelovic and I.D.Ilic, "Modelling Development of Volontary Pension Fund Using Mathematical Model Of Approximation with Lagrange Interpolation Polynomials," *Ekonomske teme*. vol. 59, no.2, pp.243-257, 2021.

[14] R. Milo, "What is the total number of protein molecules per cell volume? A call to rethink some published values," BioEssays, vol.35, no. 12, pp. 1050-1055, Dec. 2013.

Reconstruction of fiber reinforcement in epoxy-based composite

Aleksandar Stajčić, Vojislav V. Mitić, Cristina Serpa, Branislav Randjelovic, Ivana Radović

***Abstract*—Polymer matrix composites (PMCs) are very attractive materials due to a possibility to achieve versatile properties by combining with ceramic or metal reinforcement in different shapes and sizes. As a result, PMCs have found application in nearly every field, from household appliances to aerospace industry. Modern microelectronic devices contain conductive polymers with fillers that enhance their electrical properties. In addition, PMCs are being used as insulators and adhesives, contributing to the long life of electronic devices. Epoxy resins are the most commonly used insulators and adhesives. In order to improve their fracture toughness, glass fibers can be used as an efficient reinforcement. However, with the purpose of designing a composite with good mechanical properties and durability, deep knowledge of microstructure is required. In addition, microstructural analysis can be used to connect shape and size of pores or reinforcement with various physical properties. Fractal nature analysis is a valuable mathematical tool that can be employed for different shapes and forms rendering. In this manner, successful design and prediction of composite's properties could be obtained. In this research, field emission scanning electron microscopy (FESEM) images were used for fractal analysis of glass fibers, with the aim of reconstructing the shape.**

***Index terms*— Fractal analysis; Composites; Epoxy; Microelectronics.**

I. Introduction

Composites represent multiphase materials containing two or more phases distinct by an interface [1-3]. Physical properties of composites are significantly different from the initial constituents' properties [4,5]. Civilization modernization was followed by increased production and development of composites both at the research and industrial scale. With composite design and processing, structural, thermal, electrical and other properties of the constituents are improved. Synergetic effect of matrix and reinforcement properties results in lightweight materials with high toughness and strength that can be resistant to corrosion, chemicals and temperature [6]. Nowadays, there are many efficient ways to process composite with targeted functional properties, with structure control at micro- and nanoscopic level [7-12]. Polymers are very attractive as matrix materials in composites, due to their low price and density, as well as wide range of good physical and chemical properties. Conductive polymers like poly(vinylidene fluoride) polypyrrole are investigated and implemented in various electronic parts. Composites with epoxy matrix are used as insulators, offering device stability and durability [13]. Since epoxy generally has low fracture toughness, fibers are usually incorporated for the reinforcement. They increase toughness, specific strength and modulus of elasticity [14,15] In order to avoid delamination and fiber separation from the matrix, thorough insight into the structure in desirable [16-18]. Fractal nature analysis is a powerful mathematical tool for the investigation of materials morphology that is used for characterization of grains and pores [19]. However, it can also serve to describe and predict the shape and size of reinforcement, enabling more efficient future composite design. In this manner, processing-structure-property circle can be closed. FESEM images can be used for the shape and size reconstruction of the fibers.

A. Fractal nature analysis

The fractal nature exists within physical systems structures and contact surfaces, from microstructures, down to the nano-scale level, up to the global bulk and massive shapes. Fractal nature analysis presents a possible approach for the investigation of contact phenomena establishing the grain contacts models, offering ceramics and other materials structure analysis, description and prediction of grains' and pores shape, along with relations between structure and electric-dielectric properties. Contribution of fractals correction could be observed and explained on intergranular Heywang capacity model, Schottky barrier, Curie-Weiss law, Clausius-Mossotti relation and other parameters in the field of dielectric and ferroelectric materials, by introducing complex fractal correction factor α (grain and pores surface influence and Brownian particle motion). The development of fractal

A. Stajčić is with the Center of Microelectronic Technologies, Institute of Chemistry, Technology and Metallurgy – National Institute of the Republic of Serbia, University of Belgrade, Belgrade, Serbia, stajcic@nanosys.ihtm.bg.ac.rs

V. Mitić is with the University of Nis, Faculty of Electronic Engineering, Nis, Serbia and Institute of Technical Sciences, Serbian Academy of Sciences and Arts, Belgrade, Serbia vmitic.d2480@gmail.com

C. Serpa is with the ISEL - Instituto Superior de Engenharia de Lisboa do Instituto Politécnico de Lisboa cristinaserpa@hotmail.com

B Ranđelović is with the University of Nis, Faculty of Electronic Engineering, Nis, Serbia and University of K. Mitrovica, Faculty of Teachers Education, Leposavic, Serbia bane@elfak.ni.ac.rs

I. Radović is with the Department of Physical Chemistry, 'VINČA' Institute of Nuclear Sciences - National Institute of the Republic of Serbia, University of Belgrade, Belgrade, Serbia ivana_r@vinca.rs

analysis idea is inspired by self-similarity in nature biosystems, where the chaotic structures could be controlled by recognized geometry structure or just to have disorder controlled towards the order. One of the goals is to recognize and develop the bridge between biosystem of living organisms and physical systems condense matter particles. In this manner, we use the inspiration from nature for better understanding the particles physics motions, which could be observed as biomimetic system.

Every fractal object (FO) has its fractal dimension – Hausdorff dimension (D_H), a real number, smaller compared to the geometric dimension of the FO minimal space. Influence of pores' and grains' fractal dimension on materials properties has already been established [20-25]. Unlike ideal, natural fractals have scale-dependent fractal dimension [26]. Nature objects, such as water surface, air particles, trees and many others do not show intrinsic structural, but statistical self-similarity; therefore, they are considered as almost fractals. Reconstruction of such shapes requires modified mathematical approach, offered by fractal geometrical analysis. This mathematical technique can be performed on field emission scanning electron microscopy (FESEM) images, by identifying fiber phase and pores shapes and boundaries, as well as fiber-matrix bonding at the interface. In this study, fiberglass mat was used for the reinforcement of epoxy. FESEM image of enlarged fiber after the composite fracture was used for the reconstruction of data.

II. The Method

A. Fractal reconstruction of data

Fractal nature analysis of experimentally determined physical properties is performed using a novel affine fractal regression model described by the equations published in our previous research. The aim is to find coefficients that fit experimental data for the following equation system:

$$\varphi\left(\frac{x+j}{p}\right)=a_j\varphi(x)+b_jx+c_j \tag{1}$$

where x∈[0,1), 0≤j≤p-1, a_j represent fractal and b_j directional coefficients, with $0<|a_j|<1$, with domain [0,1), p stands for fractal period. Real solution equation system is called fractal function φ:[0,1)→R, having mathematical fractal structure – function graph plot represents fractal curve. Higher a_j appear in the case of strong fractal oscillations. The curve fractal level defined by the equation system is L; the first fractal level is replicated in the entire domain over every of the p sub-intervals, building the second fractal level.

In order to obtain coefficients that fit the data, explicit solution of the problem that depends on the p-expansion of numbers in [0,1) is used. For L=2, this solution is

$$\varphi(0)=\frac{c_0}{1-a_0} \tag{2}$$

$$\varphi\left(\frac{\xi_1}{p}\right)=a\xi_1\frac{c_0}{1-a_0}+c\xi_1,\xi_1\neq 0 \tag{3}$$

$$\varphi\left(\frac{\xi_1}{p}+\frac{\xi_2}{p^2}\right)=a\xi_1\left(a\xi_2\frac{c_0}{1-a_0}+c\xi_2\right)+b\xi_1\frac{\xi_2}{p}+c\xi_1,\xi_2\neq 0 \tag{4}$$

For obtaining the best coefficients, the theoretical approach computes the SSR - sum of square residuals in between the formal definition and the real values. Afterwards, the partial derivatives of SSR are equalled to zero, for minimizing the error. The best solution of the problem is given when:

$$\frac{\partial SSR}{\partial a_j}=0,\frac{\partial SSR}{\partial b_j}=0,\frac{\partial SSR}{\partial c_j}=0 \tag{5}$$

for all j=0,1,2,…,p-1. This is a problem with 3p parameters, to estimate where the equations to solve are nonlinear.

The mathematical analytical solution of this partial derivative system is not possible to compute, and a numerical approach is needed. With the software for numerical computation of the solution, called Fractal Real Finder, we worked on samples and obtained estimated curves and estimates of Hausdorff dimension. With the input of the real data, the program executes simulations and gives an output with a fractal curve as modelled above.

With the estimated fractal curves, we may estimate the Hausdorff dimension. The Hausdorff dimension is an indicator of the chaotic/irregular data behavior. The classical dimension is represented by integer: 1 for lines and curves, 2 for 2D objects, 3 for solid 3D objects. There are structures that have characteristics in between two integer dimensions. In that case, we may estimate a non-integer dimension. The fundamental theoretical mathematical non-integer dimension is Hausdorff dimension, sometimes referred as fractal dimension. The box dimension is a simplified indicator that provides estimates for the real Hausdorff dimension of real data.

Proposition. The Hausdorff dimension D of the function graph, φ solution of the above system is upper bounded by the solution of:

$$\sum_{j=0}^{p-1}\beta_j^{\,D}=1 \tag{6}$$

$$where\ \beta_j=max\left\{\frac{1}{p},|a_j|\right\},0\le p\le p-1$$

The coefficients with fractal relevance are those a_j such that $|a_j|>1/p$.

From the following image (Figure 1), we selected a centre

small part (lighter bar) and zoomed in it to a new image (Figure 2).

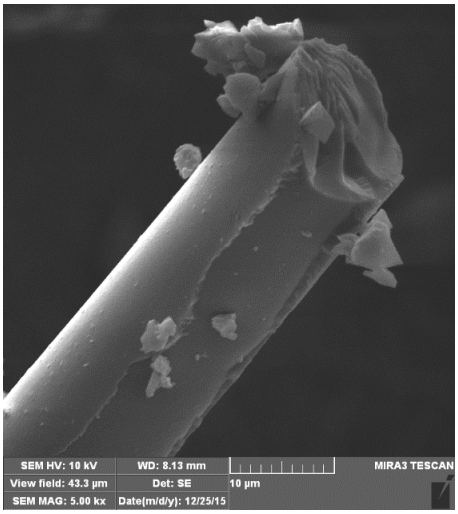

Fig. 1. FESEM of a broken glass fiber.

III. Results and Discussion

We inserted red points circling a contour of the tip of the glass fibre in a polar grid, as the following figure.

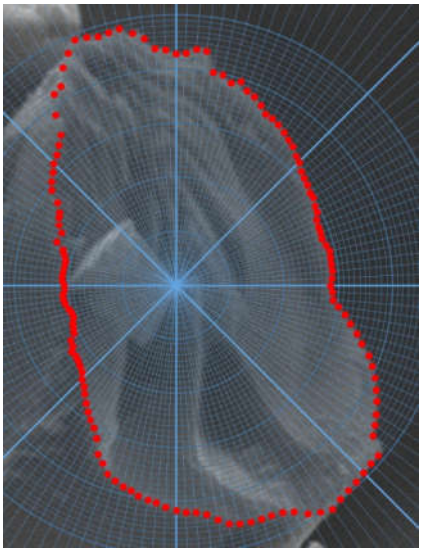

Fig. 2. Enlarged tip of the broken fiber.

We introduced red points in a border line. The fractal reconstruction is plotted in the figure next to the selected part of the image. In this case, we put the default domain in the vertical axis and upside down to match with the position of the image.

From a change of variables, from polar to cartesian variables, we run the Fractal Real Finder software for the sequence of radiuses and obtain the estimated fractal model with coefficients, as in Table below. The sequence of points is the set of radiuses corresponding to $p^L = 12^2 = 144$ angles around the image.

TABLE I
Estimated coefficients for the fractal curve of the radius

	0	**1**	**2**	**3**	**4**	**5**
a_j	0.081	-0.044	0.012	-0.002	-0.017	0.014
b_j	0.731	-2.212	-0.805	-0.098	0.603	1.362
c_j	3.951	4.989	2.695	2.118	2.156	2.852
	6	**7**	**8**	**9**	**10**	**11**
a_j	0.027	-0.057	-0.013	0.021	-0.013	0.024
b_j	0.695	-0.005	-1.654	-0.037	0.517	0.712
c_j	3.957	5.072	4.608	2.821	2.868	3.304

This fractal reconstruction reveals no fractal coefficients (those bigger than $1/p = 0.8(3)$) and, in consequence, the corresponding Hausdorff estimate is 1. Returning to polar coordinates (radius and angle), we plot the estimated curve as follows.

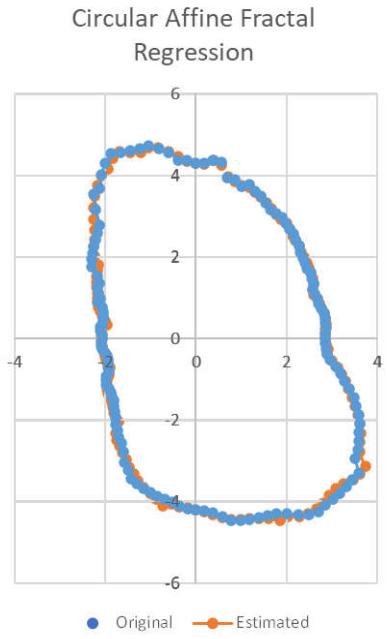

Fig. 3. Fractal curve of the fiber shape

IV. Conclusion

In this paper, fractal nature analysis was applied on fiber-reinforced composite for the reconstruction of fiber shape. The analysis with software Fractal Real Finder, fractal curve depicting the shape was obtained, as well as Hausdorff dimension of 1.21968. This indicates that the fibers have been successfully reconstructed. The finding achieved in this study

enables the use of the fractal software analysis for the design and prediction of efficient reinforcement for epoxy-based composites in the future.

ACKNOWLEDGMENT

This work was financially supported by the Ministry of Education, Science and Technological Development of the Republic of Serbia (Grant No. 451-03-68/2021-14/200017 and 451-03-68/2021-14/200026).

REFERENCES

[1] A. K. Kaw, Mechanics of Composite Materials, CRC Press, Boca Raton, 2005.

[2] D. D. L. Chung, Composite Materials: Science and Applications, Springer-Verlag London, 2010. pp 1-34.

[3] J. N. Reddy, Mechanics of Laminated Composite Plates and Shells: Theory and Analysis,CRC Press, Boca Raton, 2003.

[4] R. Aleksić, I. Živković, P. Uskoković, Kompozitni materijali, TMF Beograd, 2015.

[5] V. Radojević, R. Aleksić, Mehanička svojstva materijala, TMF Beograd, 2015.

[6] C. Shi, Y. L. Mo, Engineering Materials for Technological Needs, vol. 1, World Scientific Publishing Co. Pte. Ltd, Singapore, 2004.

[7] I. Radovic, A. Stajcic, A. Radisavljevic, F. Veljkovic, M. Cebela, V.V. Mitic, V. Radojevic, Solvent effects on structural changes in self-healing epoxy composites. *Mater.Chem. Phys*., 256 (2020) 123761.

[8] I.M. Radovic, D.B. Stojanovic, A. Kojovic, M. Petrovic, P.S. Uskokovic, V.J. Radojevic, R.R. Aleksic, Healing efficiency of polystyrene electrospunnanofibers with Grubbs' catalyst in thermosetting composite, *J. Compos. Mater*., 51 (2017) 3003–3016.

[9] A. Grujić, J.Stajić-Trošić, M. Stijepović, S.Putić, D.Nedeljković, A.Stajčić, R.Aleksić, Dynamic Mechanical Behaviour of Polymer Bonded Nd-Fe-B Composite Materials, *Mater. Trans*., 53 (2012) 395-400.

[10] A.P. Stajčić, J.T. Stajić-Trošić, A.S. Grujić, M.Z. Stijepović, N.L. Lazić, T. Žák, R.R. Aleksić, Hybrid Nd-Fe-B/barium ferrite magnetic materials with epoxy matrix, *Hem. Ind*. 66 (2012) 301–308.

[11] A. Stajcic, I. Radovic, V. Cosovic, A. Grujic, J. Stajic-Trosic, R. Jancic-Heinemann, The Influence of Barium Ferrite Nanoparticles on Morphological and Mechanical Properties of Ethyl Cellulose Based Nanocomposites, *Sci. Sinter*., 51 (2019) 277-283.

[12] D.M. Nedeljković, A.P. Stajčić, A.S. Grujić, J.T. Stajić-Trošić, M.M. Zrilić, J.S. Stevanović, S.Z. Drmanić, The Application of Zeolite Nanopowder for the Construction of the Dense Composite Polymer Membranes for Carbon Dioxide Separation, *Dig. J. Nanomater. Bios.,* 7 (2012) 269-782.

[13] K. Chen, X. Zhao, F. Zhang, X. Wu, W. Huang, W. Liu, X. Wang, Influence of gamma irradiation on the molelucular dynamixs and mechanical properties of eoxy resin, Polym. Degrad. Stab. 168 (2019) 108940.

[14] P. Zhang and G. Li, Advances in healing-on-demand polymers and polymer composites. *ProgPolymSci* 57 (2016) 32–63.

[15] A. Zucchelli, M.L. Focarete, C. Gualandi and S. Ramakrishna, Electrospun nanofibers for enhancing structural performance of composite materials. *PolymAdvTechnol* 22 (2011) 339–349.

[16] D.D.L. Chung *Composite materials: science and application.* 2nd ed. London: Springer-Verlag, 2010, p.95.

[17] S.K. Ghosh, Self-healing Materials: Fundamentals, Design Strategies, and Applications. In: Ghosh SK (ed) *Self-healing Materials: Fundamentals, Design Strategies, and Applications*, Weinheim: WILEY-VCH Verlag GmbH & Co. KGaA, 2009, pp. 1–28.

[18] M. Scheiner, T.J. Dickens and O. Okoli, Progress towards self-healing polymers for composite structural applications. *Polymer* 83 (2016) 260–282.

[19] V.V. Mitic, G. Lazovic, V. Paunovic, N. Cvetkovic, D. Jovanovic, S. Veljkovic, B. Randjelovic, B. Vlahovic, Fractal frontiers in microelectronic ceramic materials, Ceram. Int. 45 (2019) 9679-9685.

[20] R.P. Taylor, B. Spehar, Fractal Fluency, An intimate relationship between the brain and processing of fractal stimuli, in: Di Ieva A (Ed.), The Fractal Geometry of the Brain, Springer, 2016.

[21] N.C. Kenkel, D.J. Walker, Fractals in the biological sciences, COENOSES 11 (1996) 77–100.

[22] V.P. Dimri, Application of Fractals in Earth Sciences, Balkema, Rotterdam, 2000.

[23] L.G. Lanza, J. Gallant, Fractals and Similarity Approaches in Hydrology, Part 1. Theory, Organization and Scale, Published Online John Wiley and Sons, 2006.

[24] N.Cohen, Fractal antennas and fractal resonators, Patent US 6452553 B1, 1995.

[25] C.P.Baliarda. et al.,Space-filling miniature antennas, PatentUS 8207893 B2, 2000.

[26] V.V. Mitic, Lj. Kostic, V. Paunovic, G. Lazovic, M. Miljkovic, Fractal nature structure reconstruction method in designing microstructure properties, Mater. Res. Bull. 101 (2018) 175-193.

The Neural Network Application on Ceramics Materials Density

Srdjan Ribar, Vojislav V.Mitic, Branislav Randjelovic, Dusan Milosevic, Vesna Paunovic,
Hans Jorg Fecht, Branislav Vlahovic

***Abstract* — In this research back propagation neural network (BP) was applied on ceramics material samples, consolidated by sintering data obtained in analyzed experiment in a specific way. The main characteristic of BP is that it is capable to perform arbitrarily input-output data mapping due to large set of adjustable coefficients called weights. Desired mapping is possible to achieve if coefficients are set to proper value and this procedure is called training. At the beginning of training process weights are set to random values. Error is defined as a difference between desired and actual network output and weight coefficients have a contribution in generating error.**

Within experimental from material density values sintering results, measured on a surface, we investigate a possibility to calculate density within sintered structure. In this case BP training procedure is used as a tool to spread values measured on a sample surface – density. In this investigation network errors are replaced with density values obtained in ceramics sintering process. We sucesfully performed this neural network application novelty in ceramics material sciences within sintering process for the case $\rho=5.4x10^3[kg/m^3]$.

***Index Terms* — ceramics, sintering, neural network, error, density.**

I. Introduction

In this research ceramics material samples, consolidated by sintering data obtained in analyzed experiment are explored using back propagation neural network. Back propagation neural network is performing arbitrarily input-output data mapping due to large set of adjustable coefficients, Those coefficients are called weights. If coefficients are set to proper value, then desired mapping can be achieved and this procedure is called training of neural network. At the beginning of this process weights are set to random values, and during training process input-output training data is set to a network. It means that desired input-output mapping is known.

Due to inappropriate weight values mapping is performed with significant error, where error is a difference between desired and actual network output. All weight coefficients have a significant contribution in generating this error. Since this measured error is occurred due to incorrect weight values of a whole network it is necessary to change weights through the whole network in the sense to minimize it. This process starts from the output layer where error is measured and finishes in input layer. This procedure of changing weight values is called training. Training is applied on a whole training set data nummerous times. With the change of the values of the coefficients, through the training, process error decreases and after trainining process is finished further on network mapping is satisfactory even for a new input data on network has not been trained. Training process implies changing all network coefficients starting from network output through the whole network to the input. Since this process performs from network output to network input it is called error back propagataion [1,2,3,4]. So, contribution of all network elements generating output error is calculated. Training process is finished when all input-output data are mapped within predefined error.

The main idea in this paper is to extend the neural network application on processes in sintering and calcualtion of various parameters, within different sintering temperatures intervals. The process of consolidation the ceramics materials at different thermal conditions has a very important relation to density.

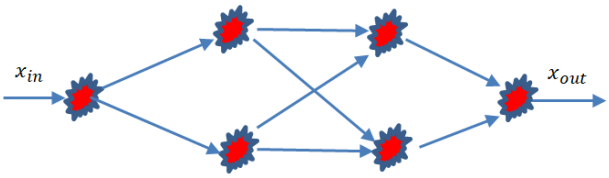

Figure1. The principle scheme neural networks.

Srdjan Ribar is with Faculty of Mechanical Engineering, University of Belgrade, Kraljice Marije 16, 11120 Belgrade Serbia, Belgrade, Serbia (e-mail: srdjanribar@gmail.com).

Vojislav V.Mitić is with Faculty of Electrical Engineering, University of Nis, 14 Aleksandra Medvedeva, 18000 Belgrade, Serbia (e-mail: vmitic.d2480@gmail.com).

Branislav M.Randjelović is with Faculty of Electrical Engineering, University of Nis, 14 Aleksandra Medvedeva, 18000 Belgrade, Serbia (e-mail: bane@elfak.ni.ac.rs).

Dusan Milosević is with Faculty of Electrical Engineering, University of Nis, 14 Aleksandra Medvedeva, 18000 Belgrade, Serbia (e-mail: dusan.milosevic@elfak.ni.ac.rs).

Vesna Paunović is with Faculty of Electrical Engineering, University of Nis, 14 Aleksandra Medvedeva, 18000 Belgrade, Serbia (e-mail: vesna.paunovic@elfak.ni.ac.rs).

Hans J. Fecht is with University of Ulm, Institute of Functional Nanosystems, Ulm, Germany (e-mail: hans.fecht@uni-ulm.de).

Branislav Vlahovic is with North Carolina Central University, (NCCU), Durham, North Carolina USA (e-mail: vlahovic@nccu.edu).

We introduce neural networks (Fig.1) as an efficient tool for application on calculation of different physical parameters. They are very useful, from experimental point of view, because their applciation on results of measurements fit much more extended experimental intervals with exeptible neglected error.

Material structure is assumed as a multi thin layers coating around the both sides grains interconnections. Any signal measured on the material surface could be propagated instead neural network error through the whole structrure. This idea was analyzed in [5,6,7] where relative capacitance measured on a sample surface was propagated through the ceramics structure assuming that ceramic structure can be presented by a neural network, Fig. 1.

Sintering material density value (in last column of Table I) is one of experimentally obtained parameters. These values are measured on a surface. Our goal is to investigate a possibility to calculate density of a sintered material within a sintered structure. In order to solve this problem a possible solution would be a usage of neural networks. Back propagation neural network (BP) seems as an appropriate tool taking into account a training procedure that changes weight coefficient values [8,9,10,11]. Weight values are changed all through whole network proportionately to an error value measured on an output network layer.

In this case BP training procedure is used as a tool to spread values measured on a sample surface – density. Various BP structures are trained to map arbitrary input-output data. During training process an absolute error value measured on an output is used to change weight values through the network. In this investigation network errors are replaced with density values obtained in sintering process, Table 1. first row $\rho=5.4x10^3[kg/m^3]$.

II. Experimental results and methods

The ceramic powder preparation for sintering consolidation for $BaTiO_3$ - ceramics samples is consisted of different steps: (a) measuring and forming a mixture of starting powders with impurities, (b) wet mixing and spraying, (c) molding and process control and (d) preparation, samples sintering and process control. We applied high purity commercial $BaTiO_3$ Murata powder [12] (mean grain size <2μm, 99.9 % purity). We analyzed the influence of sintering parameters on the final $BaTiO_3$-ceramics characteristics, onto the density. Powder mixture was processed into a mill with balls and water and organic binders were added and homogenization was about 48 hours, and the mass was transferred by a membrane pump and dried, so we got desired powder granulation. We tested the material density every hour by a special vessel and after that vibrating sieve was applied. Roughly shaped powder particles were of diameters 10-130μm.

We analized the sintering temperatures (1190-1370ºC) and time (2-3h) with impact of additive CeO_2, $MnCO_3$. For this research paper we stress the relation for pressure 86MPa and density.

TABLE I
Experimental results

sample type	***P [MPa]***	***ρ [kg/m³]***
$BaTiO_3$ – ceramics with basic mixture	86	*5.4x10³*
$BaTiO_3$ -ceramics: composition 0.1%CeO_2+0.14%$MnCO_3$	86	*3.2x10*
$BaTiO_3$ -ceramics: composition 0.1%CeO_2+0.14%$MnCO_3$	86	*3.4x10*

In further theoretical experiment we used concrete data $\rho=5.4x10^3[kg/m^3]$, from the first raw of the Table I.

A. Theoretical experiment and neural network method application

For a network with one neuron in each of two hidden layers errors calculated (Table II) in training process are

TABLE II

neuron	first hidden layer	second hidden layer	output neuron
1	*0.076786*	*0.141702*	*0.185405*

Calculated density ρ in hidden layers (Table III) is

TABLE III

neuron	first hidden layer	second hidden layer	output neuron
1	*2200*	*4300*	*5400*

Error for a network with two neurons in a first hidden layer and one neuron in a second hidden layer (Table IV) is

TABLE IV

neuron	first hidden layer	second hidden layer	output neuron
1	*0.023776*	*0.314802*	*0.887293*
2	*0.045009*		

Calculated density ρ in hidden layers (Table V) is

TABLE V

neuron	first hidden layer	second hidden layer	output neuron
1	*273,9*	*1900*	*5400*
2	*144,6*		

Error for a network with two neurons in a first hidden layer and two neurons in a second hidden layer (Table VI) is

TABLE VI

neuron	first hidden layer	second hidden layer	output neuron
1	*-0.0654*	*-0.2297*	*0.903708*
2	*-0.05848*	*-0.05259*	

Calculated density ρ in hidden layers (Table VII) is

TABLE VII

neuron	first hidden layer	second hidden layer	output neuron
1	*349*	*314*	*5400*
2	*391*	*1372*	

Error for a network with three neurons in a first hidden layer and one neurons in a second hidden layer (Table VIII) is

TABLE VIII

neuron	first hidden layer	second hidden layer	output neuron
1	*-0.04998*	*-0.10846*	*0.668582*
2	*-0.06411*	*-0.16845*	
3	*-0.03064*		

Calculated density ρ in hidden layers (Table IX) is

TABLE IX

neuron	first hidden layer	second hidden layer	output neuron
1	247	*1360*	*5400*
2	518	*876*	
3	*404*		

There is a possibility to calcularte error and ednsity using other neural networks (for example: 3 neurons in first level, 2 neurons in second level; 3 neurons in first level, 3 neurons is second level; 4 neurons in first level, 1 neuron is second level) but this will be part of some future researche.

B. Results and discussion

Obtained and trained neural networks are given on next figures.

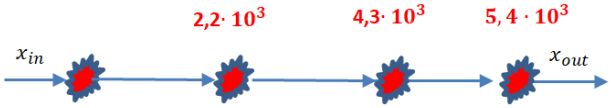

Figure 2. Neural network with one neuron per each hidden layer.

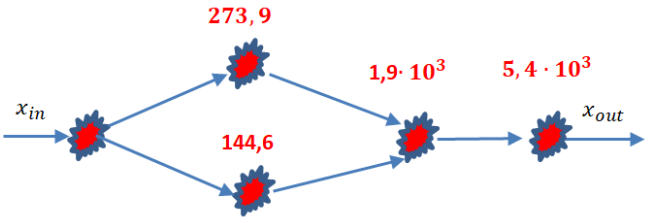

Figure 3. Neural network with two neurons in first hidden layer and one neuron in second hidden layer

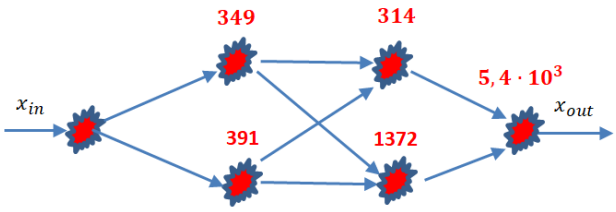

Figure 4. Neural network with two neurons per each hidden layer.

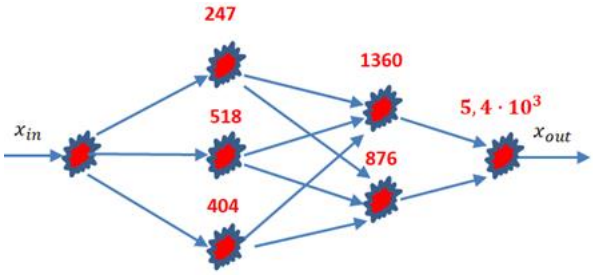

Figure 5. Neural network with three neurons in first hidden layer and two neurons in second hidden layer.

Based on experimentaly consolidated samples and applied the neural networks in three diferente cases shown on Fig.2, Fig.3 and Fig.4, we sucessfully performed this original novelty in getting the samples surface density, based on a theoretical experiment and neural networks calculations.

The advantage in this methodology is within the collecting the ceramics materials densities, from the sample surfaces, based on neural networks. This is efficient and productive way for data densities which is avoiding much more experimental activities and materials and energy and time losses.

III. CONCLUSION

In this research report we explained the neural network method and its application on some results, which are surface density on the experiment. We collected in our experiment a plenty of different results, but we consistently demonstrated this novelty with surface density ρ=*5.4x10^3[kg/m^3]*..

We presented the densities values within the different ceramics sample microstructure levels. Without this method, we could have problem to calculate the desired material density information only by stochastic mathematical approach. On this way, we have very new frontiers in science of sintering ceramics processing and technology howe can get the densities within the whole morphology.

All of this also opens new directions for predicting - designing and prognosis within the ceramics structure, where we would like to form the projective structures on a quit precise way [13,14,15,16,19].

In further experiments and researche we will show how those results, based on surface density, can be calculated on some different neural networks [16,17,18,20], with different shapes and various combination of neurons in hidden layers. We will also show how this approach can be applied for calculation of various other parameters in similar manner, based on obtained experimental results.

REFERENCES

[1] Rumelhart, D., *et al*. Learning representations by back-propagation errors, *Nature*, 323, (1986) pp. 533-536

[2] da Silva I.N., et al. Artificial Neural Network Architectures and Training Processes, in: *Artificial Neural Networks*. Springer, Cham., 2017, pp.21-28

[3] Ribar S. *et al*. Neural Networks Application on Human Skin Biophysical Impedance Characterisations, *Biophysical Reviews & Letters*, 16, (2021), pp. 2021 – 19

[4] Hecht-Nielsen: Theory of the backpropagation neural network, International Joint Conference on Neural Networks, IJCNN, Washington, D. C., USA, 1989. Vol. 1, pp 593-605

[5] Mitic V. V., *et al*. The Artificial Neural Networks Applied for Microelectronics Intergranular Relations Determination, *Integrated Ferroelectics*, 212, (2020)

[6] Mitic V. V., *et al*. Neural Networks and Microelectronics Parameters Distribution Measurements Depending on Sintering Temperature and Applied Voltage, MPL B, 34 (**35)** (2020) pp. 2150172.

[7] Randjelovic B., *et al*. "Ceramics, Materials, Microelectronics and Graph Theory new Frontiers", MPLB, Vol 34 (34) (2020) pp.2150159.

[8] Mitic V. V., *et al*. Entropy and fractal nature, *Thermal Science*, 24 (2020) 3B pp. 2203–2212.

[9] Mitic V. V., *et al*., "Butler-Volmer Current Equation and Fractal Nature Correction in Electrochemical Energy", *Thermal Science***,** (2020), p. 232-232,

[10] Randjelovic B., *et al*. "Graph Theory Approach in Synthetized Diamonds Electrophysical Parameters Defining", in: *Bioceramics, Biomimetic and other Compatible Materials Features for Medical Applications*, (Ed. Najman S., Mitic V., Groth T., Barbeck M., Yu Chen P., Sun Z.), Springer Nature, Cham, Switzerland, 2021, accepted for publication

[11] Ribar S., *et al*. "Neural Networks from Biophysical Applications in Microelectronics Parameters Measurements", in: *Bioceramics, Biomimetic and other Compatible Materials Features for Medical Applications*, (Ed. Najman S., Mitic V., Groth T., Barbeck M., Yu Chen P., Sun Z.), Springer Nature, Cham, Switzerland, 2021, accepted for publication

[12] Mitic V.V.: Structure and electrical properties of $BaTiO_3$ ceramics, (in Serbian), Zaduzbina Andrejevic, Belgrade, Serbia, 2001

[13] V.V.Mitic, B.Randjelovic, I.Ilic, S.Ribar, **C**.An-Lu, A.Stajcic, B.Vlahovic."The 3D graph approach for breakdown voltage calculation in BaTiO3 ceramics", IJMPB, Vol 35 (7) (2021) pp. 2150103.

[14] V.V.Mitic, G.Lazovic, B.Randjelovic, V.Paunovic, I.Radovic, A.Stajcic, B.Vlahovic: "Graph Theory Applied to Microelectronic Intergranular Relations", Ferroelectrics, 570 (2021) p. 145-152.

[15] V. Mitlić, G. Lazović, B.M. Randjelović, V. Paunović, J.M. Wu D.Mancić,, J.R. Hwu, "Fractal Microeletronic Frontiers and Graph Theory Applications", Int.Conference MS&T **2019**, Book of Abstracts, Portland, USA, 29 September – 03 October 2019.

[16] V. Mitić, G. Lazović, C.A.Lu, I.Radovic, V. Paunović, A. Stajcic, B.Randjelović, S.Ribar, B. Vlahovic, "Investigation of intergranular dielectric properties within the relation between fractal, graph and neural networks theories", Int.Conf. Electronic Materials and Applications EMA-2021, Virtual, January 19-21, 2021.

[17] V. Mitić, C. Serpa, C.A.Lu, V. Paunović, I.Radovic, B.Randjelović, S.Ribar, A. Stajcic, B. Vlahovic, "Fractal, graph and neural network theories applied on BaTiO3 electronic ceramics", Int.Conf. Electronic Materials and Applications EMA-2021, Virtual, January 19-21, 2021.

[18] V. Mitić, I.Radovic, C.A.Lu, S.Ribar, B.Randjelović, A. Stajcic, H. Fecht, B. Vlahovic, "Neural networks and applied graph theory approaches for intergranular properties measurements investigation", Int.Conf. Electronic Materials and Applications EMA-2021, Virtual, January 19-21, 2021.

[19] V. Mitić, C.A.Lu, B.Randjelović, V. Paunović, I.Radovic, A. Stajcic, J.Kotnik, H.Fecht, B. Vlahovic, "3D graph theory application on modified nano BaTiO3 electronic ceramics", Int.Conf. Electronic Materials and Applications EMA-2021, Virtual, January 19-21, 2021.

[20] Mitic V. V *et al.* Sinterign Temperature Influenceo on Grains Function Distribution by Neural Network Application, Thermal Science (2021) (accepted).

Structural Characterization of $La(Mg_{1/2}Ti_{1/2})O_3$ (LMT) Perovskite for Mobile communications

Kouros Khamoushi, Vojislav Mitić, Jelena Manojlović, Vesna Paunović, *Member, IEEE*, Goran Lazović

***Abstract*—The phase group and structure properties of $La(Mg_{1/2}Ti_{1/2})O_3$ (LMT) ceramics, prepared via the mixed oxide route, were examined in this research. A single-phase $La(Mg_{1/2}Ti_{1/2})O_3$ ceramic were produced at different sintering temperature from 1250ºC to 1675ºC. The heating rate was 25 ° C to the sintering temperature and the cooling rate from 2 ° C per minute to room temperature. The XRD analysis determined that LMT ceramics have a cubic crystal structure with a lattice parameter a = 0.392 nm. The theoretical density of this ceramics is 6.0846 g/cm3. These materials must be sintered from 1550-1675°C to achieve a sintering density of about 99% of theoretical density. At a temperature lower than 1500°C a density was 93% of theoretical density. The temperature coefficient of resonant frequency for LMT was -72 ppm/ºC, and the Quality factor was 34000 at a frequency of 8.07 GHz.**

Key words- Microstructure: Grain growth; single phase $La(Mg_{1/2}Ti_{1/2})O_3$; Lanthanum magnesium titanium oxide.

1. INTRODUCTION

Ceramic components made of dielectric material are important for the operation of filters and oscillators in several microwave systems, such as military radar systems, mobile communications, and satellite TV receivers. Perovskites have a cubic structure with the general formula ABO3, and many are based on BaTiO3. If barium ions are located at the corner of the cube, oxygen is located at face-centered sites, and titanium ions occupy the body-centered sites. Distortion of this sort of compound produces an electrical signal, permitting BaTiO3 to serve as a transducer [1]. The size of the ions has an important share in the stability of the crystal structure, and low distortions can result in lower symmetry and drastically change the property of the compound [2]. An important class of perovskites is multiferroic, which simultaneously shows ferromagnetic, ferroelectric, and ferroelastic parameters in the same segment. Another advantage of perovskite compound is in medical imaging which they can be ten times more sensitive when is used for X-ray detector [3].

In microwave communications, a dielectric resonator filter is used to discriminate between wanted and unwanted signal frequencies in the transmitted and received signal. When the wanted frequency is extracted and detected, it is necessary to maintain a strong signal nevertheless. For clarity, it is also critical that seasonal temperature changes do not affect the expected signal frequencies, and resonator materials for practical application should have reliable properties. A high relative dielectric constant is needed so that the materials can be miniaturized, and a high-quality factor (Q) for improved selectivity. Low-temperature variation of the material's resonant frequency is also required so that the microwave circuits remain stable. Everything from the electromagnetic properties to the microstructure of the material is important for the result.

The gain to reduce the size, load, and expense of microelectronic tools rules for tuning τ_f in multipart perovskites have already been created, accompanied by the piezoelectric materials the most leading material is $Pb(Zr_x Ti_{1-x})$ or PZT which have much application in ultrasound transducer ceramics which used also as capacitor [4,5] according to the work [6] that τ_ε in Ba- and Sr-based complex perovskites are profoundly connected to the start and degree of octahedral tilting. Moreover, it can be tuned through ±300 MK^{-1} without significantly adjusting Q or dielectric constant (ε_r) by manipulating the perovskite tolerance factor, *t*,

$$t = \frac{R_A + R_O}{\sqrt{2}\,(R_B + R_O)} \qquad (1)$$

from 1.01 - 0.93, where R_A, R_B, and R_O are the radii of the ions in the perovskite (ABO_3) structure. Reducing *t* results in the initiation of octahedral tilt modifications. The link between τ_ε and τ_f is:

$$\tau_f = -\left(\tau_\varepsilon / 2 + \alpha_L\right) \qquad (2)$$

Kouros Khamoushi - Natural Science, Tampere University, P.O. Box 1001 FI-33014Tampere, 33720/ Finland, (Email:kouros.khamoushi@tuni.fi).

Vojislav Mitić - University of Niš, Faculty of Electronic Engineering,, Aleksandera Medvedova 14 Niš 18000 Serbia**,** **(**Email: vmitic.d2480@gmail.com**).**

Jelena Manojlović- University of Niš, Faculty of Mechanical Engineering,, Aleksandera Medvedova 14 Niš 18000 Serbia, **(**Email: jmanojlo@gmail.com)

Vesna Paunović – University of Niš, Faculty of Electronic Engineering, Aleksandra Medvedeva 14, 18000 Niš, Srbija (email: vesna.paunovic@elfak.ni.ac.rs).

Goran Lazović- University of Belgrade, Faculty of Mechanical Engineering, Serbia, (email: goran.lazovic@gmail.com)

where α_L is the coefficient of linear thermal expansion (≈10 MK^{-1} for perovskites).

$La(Mg_{1/2}Ti_{1/2})O_3$ is a perovskite formed in the pseudocubic system, although the exact crystal structure has not been fully elucidated. Its tolerance factor is t = 0.95, which, approves to the work [7], reveals the existence of both in-phase and anti-phase tilting of oxygen octahedra. The impacts of this tilting have been detected by XRD in the form of ½(111) ordering at 1600ºC sample.

Superlattice reflections corresponding to anti-phase and in-phase tilting, respectively. Systematic cation displacement was also detected by the presence of ½(210) and ½(111) reflections were observed and attributed to the expansion of the unit cell caused by the B-site cation changes. It is possible by the present tilts to reveal two possible orthorhombic space groups (Pbmn or $P2_1/n$) for the structure, but Walsenburg photographs or TEM work would be required to establish the structure.

Structurally, tilting of octahedra has similar effects as cation ordering in 1:1 type complex perovskites. Both result in expanding unit cells [8] even though cation order also reduces the space available in which the A-site cation types can rattle, it depends on the radii size of rear earth elements used in the compound. In this study, the structural characteristic of $La(Mg_{1/2}Ti_{1/2})O_3$ (LMT) in various sintering temperatures for the application of mobile phones and telecommunications was investigated.

2. Experimental Procedure

In this work, conventional mixed oxide powder processing techniques were used for the preparation of samples. A detailed description of the laboratory procedure for sample preparation is given in references [9] and [10]. Starting materials included La_2O_3 (99.9% Meldform Rare Earths, U.K), TiO (99.8% Alfa Aesar, U.K.), and $(MgCO_3)_4Mg(OH)_25H_2O$ (99% Aldrich Chemical Company, Inc, USA). La_2O_3, the rare-earth oxide, was first purposely hydrated in distilled water to form $La(OH)_3$. These hydrates were then used in the subsequent processing method, which involved milling stoichiometric quantities of powders together in a porcelain mill pot partly filled with ZrO_2 media and distilled water for four hours.

A small amount (1wt%) of Dispex A40 (Allied Colloids, Bradford, U.K.) was added as a deflocculant. The slurries were then dried overnight at 80°C. Dried powders were subsequently granulated with a mortar and pestle and sieved to under 250 µm. Calcination was achieved using a two-stage process. First, the powder was heated to 650 ºC for 2 hours in an open Al_2O_3 crucible to ensure dihydroxylation of the $La(OH)_3$. The completion of the dihydroxylation reaction was monitored by measuring the weight loss at this stage of the process. Second, this same powder was combined by hand, a lid was placed over the crucible, and it was re-heated to 1400ºC for 2 hours. Afterward, the powder was re-milled for a further four hours with 2wt% PEG 1500 (Whyte Chemicals, London) being added in an aqueous solution 5-15 min before completion. These slurries were then dried and granulated as above and subsequently pressed (125 MPa) into cylindrical pellets 10 mm in diameter and 3 mm thick. Sintering was conducted in closed alumina boats for 6 hours at temperatures ranging from 1125°C to 1675°C. Pellets were weighed up before and after sintering to quantify the degree of deficiency. Dense and homogeneous ceramic powder of lanthanum magnesium titanium oxide was obtained after pressing powder 125 MPa and sintering at 1600°C for 6 hours.

Phase groupings were verified by scanning electron microscopy (JSM 6300, Jeol, Tokyo) and x-ray diffraction (D50000, Siemens, Germany), using CuKa radiation. Some samples underwent thinning by ion milling (model 600, Gatan, California, USA) for observation in the transmission electron microscope (JEM 2010, Jeol, Tokyo).

3. Results and Discussion

Figure 1 shows the change in density of La $(Mg_{1/2}Ti_{1/2})O_3$ ceramics as a function of sintering temperature. The density of LMT ceramics increased with increasing sintering temperature and reached (87% TD) at 1250°C. Until the sintering temperature of 1300°C, the densities do not change, and then increases to (98% TD) at 1500°C. At this temperature, high-quality, high-density material is obtained.

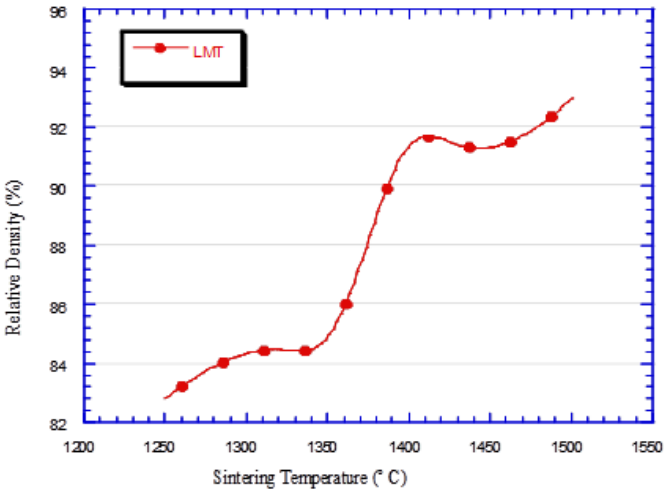

Fig. 1. Relative density of LMT samples in function of sintering temperature (Tsin=1250-1500 ºC).

XRD patterns of LMT samples, sintered at 1400-1675ºC temperature, were shown in Fig 2. Eleven samples were selected, and starting sample was sintered at 1400 ºC for 6 hours and this sintering process continued for each individual sample by increasing 25 ºC to the previous temperature. This successive test continued for every sample and ended at 1675ºC. All the samples show perovskite crystal structure. Peaks from 1400-1675ºC match the LMT structure. All the peaks match PDF card numbers 49-242. Crystallography

search match indicates that crystal structures of samples are cubic with a space group of Pa3.

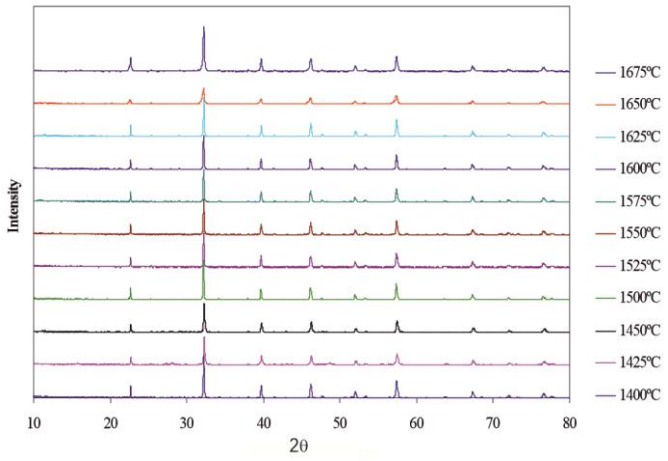

Fig. 2. X-ray diffraction (XRD) of LMT for sintering temperature of 1400-1675ºC.

The SEM image of $La(Mg_{1/2}Ti_{1/2})O_3$ is shown in Figure 3. The image shows an LMT sample sintered at 1650°C. As can be seen from Figure 3, the sample is a single-phase high-dense ceramics. The material with the second phase must show a different contrast. The background scattered image of these samples showed no differences. If the samples show two different colors in contrast, then the investigated material is not single-phase and has impurities. However, several samples of LMT were tested, and all results show pure and very dense LMT material. Also, these samples are characterized by polygonal grains the size ranging from 1 to 6μm.

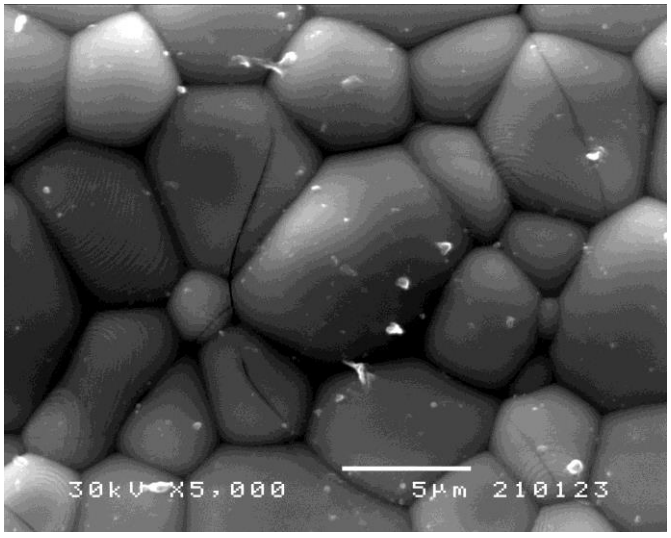

Fig. 3. SEM microphotography of LMT ceramics, sintered at 1650 °C, beam direction [111].

3.1. STRUCTURE OF $La(Mg_{1/2}Ti_{1/2})O_3$

The X-ray pattern for LMT powder shown in figure 4. It is indexed according to the Magnesium Lanthanum Titanium Oxide PDF card number 49-242 with single phase cubic crystal structure with $a \approx 0.3.92$ nm. XRD of sample powder did not show any broadening or splitting of cubic peaks. All the XRD taken from sample of calcined as well as the sintered pellets were similar.

Nevertheless, to avoid the uncertainty for the definition of the exact crystal structure and space group of LMT samples, high resolution transmission electron microscopy and Rietveld refinement by using GSAS should be performed, this work is under consideration for future.

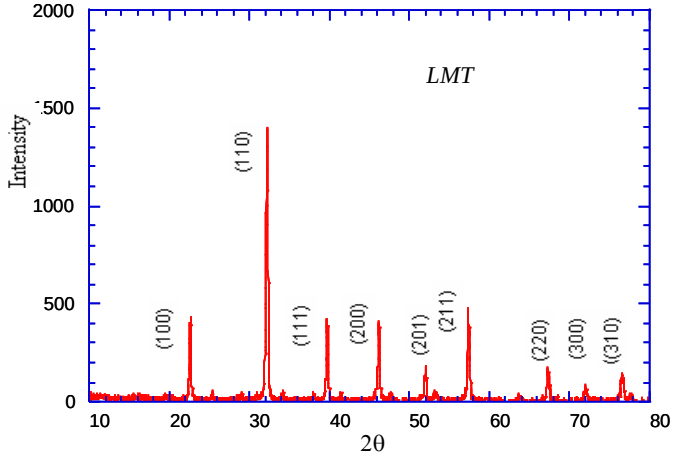

Fig. 4. X-ray diffraction pattern of $La(Mg_{1/2}Ti_{1/2})O_3$ powder after sintered at 1600°C. All the peaks have been indexed according to PDF card numbers 49-242

The temperature coefficient of the microwave resonant frequency (τ_f) and the quality factor (Q) at the resonant frequency were made from the dielectric characteristics.

The results of Q × f measurements illustrate that LMT ceramics have quality factors Q × f = 34,000 at frequency 8.07 GHz. The temperature coefficient of the resonant frequency of LMT is τ_f= -72 ppm/ ºC.

4. CONCLUSIONS AND FUTURE WORK

In this paper the structure characteristics of $La(Mg_{1/2}Ti_{1/2})O_3$ were explored. LMT has lattice parameter a = 0.392 nm and it shows a cubic crystal structure. The theoretical density is 6.0846 g/cm^3. This material can be sintered from 1550-1675 ºC to achieve sintering density of about 99% (1550ºC and 1600ºC). At lower temperature the density was under 97% that of theoretical density. The temperature coefficient of resonant frequency for LMT was -72 ppm/ ºC. The quality factor for LMT was 34000 where saturated at frequency 8.07 GHz. Clearly these materials show a good potential as filters for mobile microwave telecommunications.

Acknowledgements:

This work has been supported by Queen Mary University of London, UK, Tampere University of Technology, Finland, and the Ministry of Education, Science and Technological Development of the Republic of Serbia (Ev. No. 451-03-9 / 2021-14 / 200102).

REFERENCES

[1] K. A. Muller and T. W. Kool, properties of Perovskite and other oxide, world Scientific Publishing, Singapore (2010).

[2] H. Tanaka, H. Tabata, K. Ota, T. Kawai, "Molecular dynamics prediction of structural anomalies in ferroelectric and dielectric $BaTiO_3$-$SrTiO_3$-$CaTiO_3$ solid solutions" Physical ReviewVol.53, no 21, p. 14112-14113, 6th Ed. (1996).

[3] YC Kim, KH Kim, DY Son, DN Jeong, JY Seo, YS Choi "Printable organometallic perovskite enables large-area, low-dose X-ray imaging,", Nature, 550, 87 (2017).

[4] C. Rossel1, M. Sousa1, S. Abel1, D. Caimi, A. Suhm , J. Abergel,G. Le Rhun, and E. Defay. Defay. "Temperature dependence of the transverse piezoelectric coefficient of thin films and aging effects" Journal of Applied Physics, 115, 034105 (2014).

[5] Yingfen Wei, Pavan Nukala, Mart Salverda, Sylvia Matzen, Hong Jian Zhao, Jamo Momand,Arnoud S. Everhardt, Guillaume Agnus, Graeme R. Blake, Philippe Lecoeur, Bart J. Kooi, Jorge Íñiguez, Brahim Dkhil, "A rhombohedral ferroelectric phase in epitaxially strained Hf0.5 Zr0.5O2 thin film "Journal of Nature materials (2018) 17,pages 1095–1100 (2018).

[6] Kouros. Khamoushi, Vojislav. V. Mitic "Comparison between crystal structire and dielectric properties $Nd(Mg_{1/2}Ti_{1/2})O_3$ (NMT) and $Nd(Zn_{1/2}Ti_{1/2})O_3$ (NZT)," In process accepted on 11.5.2021 Journal of Modern Physics Letters B, (2021).

[7] D.Y.Lee S.J.Yoon, J.H.Yeo, S.Nahm,J.H.Paik, K.C.Whang, and B.G.Ahn,"Crystal structure and Microwave Dielectric properties of La(Mg½ Ti½)O3 ceramics," Journal of Materials Science Letter, vol.19 pp131-134(2000).

[8] M.P Seabra, A N Salak, M Avdeev and M Ferreira., "Structure and dielectric characterization of the $La(Mg½Ti½)O_3$-$Nd(Mg½ Ti½)O_3$ system," Journal of Physics Condensed Matter,", 15, (2003).

[9] R. Ubic, K. Khamoushi, Hu, and Isaac Abrahams, "Structure and properties of La(Mg0.5 Ti0.5)O3," Journal of European Ceramic Society, No.26, 1787-1790 (2005).

[10] R. Ubic, K. Khamoushi, D. Iddles, T. Price, "Processing and dielectric properties of $La(Mg_{0.5}Ti_{0.5})O_3$ and Nd $Mg_{0.5}Ti_{0.5})O_3$," Ceramic transaction, 167, 21-3, (2004)